A medium-independent variational macroscopic theory of two-phase porous media – Part II: Applications to isotropic media and stress partitioning. Bridging the gap between Biot's and Terzaghi's perspectives

Roberto Serpieri, Francesco Travascio

A medium-independent variational macroscopic theory of two-phase porous media – Part II: Applications to isotropic media and stress partitioning. Bridging the gap between Biot's and Terzaghi's perspectives

Roberto Serpieri*[1], Francesco Travascio[2]

[1]Dipartimento di Ingegneria, Università degli Studi del Sannio, Piazza Roma, 21 - I. 82100, Benevento, Italy. e-mail: roberto.serpieri@unisannio.it

[2]Biomechanics Research Laboratory, University of Miami, Department of Industrial Engineering, 1251 Memorial Drive, MEB 276, Coral Gables, FL, 33146, USA, e-mail: f.travascio@miami.edu

Keywords: Terzaghi's law, effective stress, VMTPM, least action principle, liquefaction

Abstract

Stress partitioning in multiphase porous media is a fundamental problem of solid mechanics, yet not completely understood: no unanimous agreement has been reached on the formulation of a stress partitioning law encompassing all observed experimental evidences in two-phase media, and on the range of applicability of such a law.

A most celebrated stress partitioning law, based on the notion of 'effective stress', is known as 'Terzaghi's principle'. However, while there is agreement on its reliability in describing the behaviour of soils and soft hydrated biological tissues, experimental observations on certain porous media have been generally interpreted as deviations from such law.

The objective of this study is to perform an analysis on the range of applicability of the notions of effective stress and effective stress principles. This is carried out employing a

*Corresponding author

variational macroscopic theory of porous media (VMTPM) derived in the companion Part I of this study. Such theory predicts that the external stress, the fluid pressure, and the stress tensor workassociated with the macroscopic strain of the solid phase are partitioned according to a relation formally compliant with Terzaghi's law, irrespective of the microstructural and constitutive features of a given medium.

Herein, these laws are applied to the study of stress partitioning in three classes of materials: linear media, media with solid phase having no-tension response, and cohesionless granular media.

It is shown that VMTPM recovers for the dynamics of isotropic media equations having the same structure of Biot's equations. Also, compliance with Terzaghi's principle can be rationally derived as the peculiar behavior of the specialization of VMTPM recovered for cohesionless granular media, in absence of incompressibility constraints. Moreover, it is shown that the experimental observations on saturated sandstones, generally considered as proof of deviations from Terzaghi's law, are predicted by VMTPM. In addition, a rational deduction of the phenomenon of compression-induced liquefaction in cohesionless mixtures is reported: such effect is found to be a natural implication of VMTPM when unilateral contact conditions are considered for the solid above a critical porosity. Finally, a characterization of the phenomenon of crack closure in fractured media is inferred in terms of macroscopic strain and stress paths.

Altogether these results exemplify the capability of VTMPM to describe and predict a large class of linear and nonlinear mechanical behaviors observed in two-phase saturated materials. As a conclusion of this study, a generalized statement of Terzaghi's principle for multiphase problems is proposed.

1 Introduction

In fluid saturated porous media, the mechanism by which external stresses are partitioned between solid and fluid phases is complex and yet not completely understood [1–10].

In the first decades of the last century, Terzaghi introduced the concept of 'effective stress', which regulated observable effects in saturated soils, according to a so called 'effective stress principle' [1, 2]. Ever since its conception, the effective stress has stimulated a large body of theoretical and applied researches in several fields dealing with the problem of stress partitioning in multiphase media [8, 9, 11–19].

The effective stress expressions so far proposed can mostly be cast in the form of relations equating the external stress applied to the medium to a linear combination of the elastic deformation in the solid skeleton and of the interstitial pressure of the fluid saturating the mixture. However, there is a certain disagreement on the coefficients to be adopted, and several different expressions have been proposed [2, 3, 5, 11, 20–24]. Comparing different expressions of stress partitioning to one another is difficult since they often derive from different multiphase poroelastic theories which proceed from substantially different physical-mathematical, or engineering, premises to introduce macroscopic stress measures [3,7,8,20,21,25–32] and from different governing balance equations [6, 11, 33–36]. Also, there is a certain disagreement on the theoretical accuracy and domain of veracity of the Terzaghi's relation. In fact, as discussed in [4, 5], no theory of poroelasticity has been able to recover a stress partitioning law for two-phase media in agreement with Terzaghi's postulated one, which can be applied to any biphasic system in absence of specific microstructural or constitutive assumptions and to any experimental condition.

The fulfillment of *medium independence* for stress partitioning within two-phase continuum poroelasticity theories, framed into the more general problem of the derivation of medium-independent continum governing equations and boundary conditions, is examined in the companion Part I of this study [37]. Therein, a rational derivation of medium-independent stress partitioning laws is obtained downstream of a purely-variational and purely-macroscopic deduction of the complete set of momentum balance equations and boundary conditions for the two-phase poroelastic problem in a *minimal* kinematic setting based on an *extrinsic/intrinsic* split of volumetric strain measures previously investigated by the authors [10, 38–43]. The theoretical frame adopted is termed Variational Macroscopic Theory of Porous Media (VMTPM). The stress par-

titioning law obtained states that the external stress tensor is always partitioned between solid and fluid phases by a relation formally coincident with the classical tensorial statement of Terzaghi's effective stress principle. In such relation, the role of the *effective stress* tensor is played by the solid extrinsic stress tensor $\check{\boldsymbol{\sigma}}^{(s)}$. Notably, this stress law has been derived in absence of any constitutive and/or microstructural hypothesis on the phases, and for this reason it has a general medium-independent validity.

However, well-known experimental results deriving from testing of saturated porous media [4, 5, 21] are usually interpreted as evidences of deviations from Terzaghi's law for specific classes of two-phase media. The primary objective of this contribution is to demonstrate that VMTPM is capable of predicting such experimental results. The other objectives are: 1) to show that VMTPM can recover results of consolidated use in poroelasticity, such as Terzaghi's stress partitioning principle and Biot's equations; and 2) to show the validity of VMTPM beyond the linear-elastic range.

Accordingly, stress partitioning laws are herein investigated for three classes of isotropic media with volumetric-deviatoric uncoupling subjected to infinitesimal deformations: 1) linear media; 2) media with no-tension response for the solid phase (yet, linear in compression); 3) cohesionless granular media. This is done by analyzing VMTPM predictions for two-phase mixtures in four thought-experiment compression tests, characterized by different loading and drainage conditions.

The paper is organized as follows. Governing equations and boundary conditions defining the two-phase medium-independent boundary-value poroelastic problem in linearized kinematics, as framed in VMTPM, are recalled from Part I in Section 2, together with the relevant medium-independent stress partitioning laws. In Section 3 this boundary-value description is specialized to isotropic media with volumetric-deviatoric uncoupling, presenting the relevant elastic moduli (Section 3.1), the corresponding governing PDEs (showing the recovery of Biot's equations) (Section 3.2) and also reporting useful Composite Spheres Assemblage (CSA) homogenization estimates (Section 3.4). The isotropic boundary-value description is deployed in Section 4 to analyze the stress partitioning response in terms of strain and stress paths in the planes of normalized strain and stress volumetric coordinates in four types of ideal compression tests: a Jacketed Drained test (JD), an Unjacketed test (U), a Jacketed Undrained test (JU), and

a (so-called) Creep test with constant confining stress and Controlled Fluid Pressure (CCFP), for three classes of isotropic media assuming volumetric-deviatoric uncoupling and infinitesimal deformations: 1) linear media; 2) media with solid phase having no-tension response; 3) cohesionless granular media. Next, in Section 5, the elemental responses analyzed in Section 4 are employed to identify the specific set-up boundary conditions used in experimental compression tests on porous water-saturated Weber sandstone [21], and analyze stress partitioning in these experiments. In Section 6 the results of Sections 4 and 5 are reconsidered in a comprehensive discussion on the range of validity of Terzaghi's effective stress principle and on the meaningfulness of the concept of effective stress. Conclusive remarks are finally reported in a final dedicated section. Details on the notation and the list of symbols used in the present paper, with related descriptions are reported in Appendix, Section 8.

2 Two-phase medium-independent boundary value VMTPM problem

The statement of the boundary value problem as derived in Part I [37] is hereby recalled. The framework adopted is medium-independent: it does not require any specific constitutive or microstructural hypotheses on the media, and neglects microinertia terms. The kinematically-linear equations are considered to describe the problem for infinitesimal deformations. It is important to remark that kinematic linearization is the only simplificative restriction applying to the equations recalled in this subsection. Conversely, no restrictions are applied with respect to constitutive nonlinearity: the equations remain ordinarily applicable to describe any nonlinear constitutive response of constituent phases. Accordingly, the deformation is described by the infinitesimal displacement fields of the solid phase $\bar{\mathbf{u}}^{(s)}$, of the fluid phase $\bar{\mathbf{u}}^{(f)}$, and by the infinitesimal intrinsic strain field $\hat{e}^{(s)}$. The scalar field $\hat{e}^{(s)}$ is a primary kinematic descriptor which corresponds to the specialization to infinitesimal kinematics of the finite macroscopic field of intrinsic volumetric strain $\hat{J}^{(s)}$. Field $\hat{J}^{(s)}$ is a finite-deformation primary descriptor in VMTPM corresponding to the ratio $\hat{\rho}^{(s)}/\hat{\rho}_0^{(s)}$ between *true* densities of solid before and after deformation. Such field can be also operatively defined by its experimental characterization in terms of

changes of solid volume fractions before ($\Phi_0^{(s)}$) and after deformation ($\phi^{(s)}$), viz.:

$$\hat{J}^{(s)} = \frac{\hat{\rho}^{(s)}}{\hat{\rho}_0^{(s)}} = \bar{J}^{(s)} \frac{\phi^{(s)}}{\Phi_0^{(s)}} \tag{1}$$

with $\bar{J}^{(s)} = \det \partial \bar{\boldsymbol{\chi}}^{(s)} / \partial \mathbf{X}$ denoting the Jacobian of the macroscopic placement field of the solid phase. In linearized kinematics, relation (1) specializes to:

$$\hat{e}^{(s)} = \frac{d\phi^{(s)}}{\phi^{(s)}} + \frac{\partial \bar{u}_i^{(s)}}{\partial x_i} \tag{2}$$

and links the characterization of $\hat{e}^{(s)}$ (see Part I of this study) to the measurement of infinitesimal porosity changes $d\phi^{(s)}$.

The kinematic descriptor fields $\bar{\mathbf{u}}^{(s)}$, $\bar{\mathbf{u}}^{(f)}$ and $\hat{e}^{(s)}$ are defined over the domain of the mixture $\Omega^{(M)}$ which, due to the infinitesimal kinematics, represents both undeformed and deformed configurations. The undeformed configuration is also defined by the fields of solid and fluid volume fractions (i.e., $\phi^{(s)}$ and $\phi^{(f)}$). The domain $\Omega^{(M)}$ is partitioned in two subsets defined as follows: $\Omega^{(f)}$ containing only fluid ($\phi^{(f)} = 1$), and the complementary subset $\Omega^{(s)} \subset \Omega^{(M)}$ where $\phi^{(s)} \neq 0$.

In the kinematically linearized theory, the macroscopic strain of the solid is defined by $\hat{e}^{(s)}$ and by the infinitesimal extrinsic strain tensor:

$$\bar{\boldsymbol{\varepsilon}}^{(s)} = \text{sym} \left(\bar{\mathbf{u}}^{(s)} \otimes \nabla \right) \tag{3}$$

while infinitesimal volumetric strain measures are the *extrinsic* volumetric strains of solid and fluid:

$$\bar{e}^{(s)} = \frac{\partial \bar{u}_i^{(s)}}{\partial x_i} = \text{tr}\bar{\boldsymbol{\varepsilon}}^{(s)}, \qquad \bar{e}^{(f)} = \frac{\partial \bar{u}_i^{(f)}}{\partial x_i} \tag{4}$$

plus the intrinsic volumetric strains $\hat{e}^{(s)}$ and $\hat{e}^{(f)}$.

The complete saturation hypothesis reads in the infinitesimal case:

$$\phi^{(s)} + \phi^{(f)} = 1, \qquad d\phi^{(s)} + d\phi^{(f)} = 0 \tag{5}$$

and, as shown in Part I, it implies the following dimensionless saturation relation between volu-

metric infinitesimal strains:

$$\phi^{(s)}\hat{e}^{(s)} + \phi^{(f)}\hat{e}^{(f)} = \frac{\partial \phi^{(s)}\bar{u}_i^{(s)}}{\partial x_i} + \frac{\partial \phi^{(f)}\bar{u}_i^{(f)}}{\partial x_i} \tag{6}$$

whereby $\hat{e}^{(f)}$ can be treated as a derived field depending from $\bar{\mathbf{u}}^{(s)}$, $\bar{\mathbf{u}}^{(f)}$ and $\hat{e}^{(s)}$.

The primary stress measures are the fluid pressure p, the extrinsic stress tensor of the solid phase $\check{\boldsymbol{\sigma}}^{(s)}$, and the intrinsic pressure of the solid phase $\hat{p}^{(s)}$. These quantities are defined by work association:

$$\check{\sigma}_{ij}^{(s)} = \frac{\partial \bar{\psi}^{(s)}}{\partial \bar{\varepsilon}_{ij}^{(s)}}, \qquad \hat{p}^{(s)} = -\frac{\partial \bar{\psi}^{(s)}}{\partial \hat{e}^{(s)}}, \qquad p = -\frac{\partial \hat{\psi}^{(f)}}{\partial \hat{e}^{(s)}} \tag{7}$$

where $\bar{\psi}^{(s)}$ and $\bar{\psi}^{(f)}$ are the macroscopic strain energy densities, and $\hat{\psi}^{(f)}$ is defined by the relation $\bar{\psi}^{(f)} = \phi^{(f)}\hat{\psi}^{(f)}$.

Momentum balances are obtained by applying a kinematic linearization to the stationarity conditions stemming from the least-Action principle. Hereby we consider the most general medium-independent equations obtained ruling out microinertia terms:

Linear momentum balance of the solid phase:

$$\frac{\partial \check{\sigma}_{ij}^{(s)}}{\partial x_j} - \phi^{(s)}\frac{\partial p}{\partial x_i} + \bar{b}_i^{(sf)} + \bar{b}_i^{(s,ext)} = \bar{\rho}^{(s)}\ddot{\bar{u}}_i^{(s)} \tag{8}$$

Linear momentum balance of the fluid phase:

$$-\phi^{(f)}\frac{\partial p}{\partial x_i} + \bar{b}_i^{(fs)} + \bar{b}_i^{(f,ext)} = \bar{\rho}^{(f)}\ddot{\bar{u}}_i^{(f)} \tag{9}$$

Intrinsic momentum balance:

$$\hat{p}^{(s)} - \phi^{(s)}p = 0 \tag{10}$$

where $\bar{\mathbf{b}}^{(sf)} = -\bar{\mathbf{b}}^{(fs)}$ are the volume forces representing the internal short-range solid-fluid interaction, $\bar{\mathbf{b}}^{(f,ext)}$ and $\bar{\mathbf{b}}^{(s,ext)}$ are external volume forces, $\bar{\rho}^{(s)}$ and $\bar{\rho}^{(f)}$ are solid and fluid apparent mass densities.

Equations (8), (9) and (10) express stationarity of the Action in relation to the displacement fields of the solid phase, of the fluid phase, and to the intrinsic volumetric strain, respectively.

When inertia terms are negligible Equations (8), (9) and (10) specialize as follows:

$$\frac{\partial \check{\sigma}_{ij}^{(s)}}{\partial x_j} - \phi^{(s)} \frac{\partial p}{\partial x_i} + \bar{b}_i^{(sf)} + \bar{b}_i^{(s,ext)} = 0 \tag{11}$$

$$-\phi^{(f)} \frac{\partial p}{\partial x_i} + \bar{b}_i^{(fs)} + \bar{b}_i^{(f,ext)} = 0 \tag{12}$$

$$\hat{p}^{(s)} - \phi^{(s)} p = 0 \tag{13}$$

Boundary conditions with bilateral contact

The achievement of bilateral contact conditions at the boundaries can be determined by gluing the external surfaces of the specimen with the internal surfaces of the environment, or by applying a compressive prestress across the boundaries. Stress-type bilateral boundary conditions over $\partial\Omega^{(M)}$ are also obtained from a variational deduction [37], and turn out to be:

$$\left(\check{\sigma}_{ij}^{(s)} - p\delta_{ij}\right) n_j = t_i^{ext} \qquad \text{over } \partial\Omega^{(M)} \tag{14}$$

where $\mathbf{n}$ denotes as usual the unit outward normal to the boundary. Boundary conditions of displacement-type are:

$$\bar{u}^{(s)} = \bar{u}^{(f)} = u^{(ext)} \qquad \text{over } \partial\Omega^{(M)} \tag{15}$$

Conditions over free solid-fluid macroscopic interfaces

In several mixture problems, such as in unjacketed tests, it is necessary to consider the condition which characterizes those interior macroscopic surfaces which, although not belonging to the true boundary $\partial\Omega^{(M)}$, are part of the boundary $\partial\Omega^{(s)}$ of the macroscopic physical subdomain $\Omega^{(s)}$ where $\phi^{(s)} \neq 0$. Such surfaces have been termed *free solid-fluid macroscopic interfaces*, see [37]. Their mathematical definition is $\mathcal{S}^{(sf)} = \partial\Omega^{(s)} \setminus \partial\Omega^{(M)}$. In points interior to $\Omega^{(s)}$ a mixture of solid and fluid is present (being both $\phi^{(s)} \neq 0$ and $\phi^{(f)} \neq 0$), while, in the external points belonging to $\Omega^{(f)}$, space is entirely occupied by the fluid alone, $\phi^{(f)} = 1$.

The following condition holds over $\mathcal{S}^{(sf)}$ [37]:

$$\check{\sigma}_{ij}^{(s)} n_j = 0 \qquad \text{over } \mathcal{S}^{(sf)} \tag{16}$$

It is worth remarking that the condition $\check{\boldsymbol{\sigma}}^{(s)}\mathbf{n} = \mathbf{o}$ over $\mathcal{S}^{(sf)}$ does not entail absence of mechanical interaction between the solid phase interior to $\Omega^{(s)}$ and the fluid external to $\Omega^{(s)}$ in the points of $\mathcal{S}^{(sf)}$, since, in these points, coupling between the solid and the surrounding fluid regions of $\Omega^{(f)}$ still remains mediated by the intrinsic stress entering (10). Hence condition (16), although formally similar, has not to be confused with the condition which in single-phase elasticity involves the Cauchy stress tensor $\boldsymbol{\sigma}^{(s)}$ holding in a point of the boundary surface of a solid domain (i.e., $\boldsymbol{\sigma}^{(s)}\mathbf{n} = \mathbf{o}$). This last condition states instead that there is no mechanical interaction between the interior solid and the external environment at that point.

Boundary conditions with unilateral contact

The typical condition for several tests on different classes of fluid saturated materials is more properly described by unilateral contact since, in most experimental setups, specimens are ordinarily not bilaterally constrained to the walls of the confining chamber [44, 45].

Unilateral contact in a point $\mathbf{x} \in \partial\Omega^{(M)}$ is addressed by combining bilateral (*closed contact*) boundary conditions, corresponding to full adhesion between the solid macroscopic external surface and the container wall boundaries expressed, with *open contact* conditions, corresponding to the solid phase boundary moving off the wall boundaries. Closed contact conditions are expressed by equations (14) and (15) (with $u^{(ext)}$ representing the displacement of the container-wall boundary). In open contact conditions, the solid macroscopic external surface upon moving off the wall boundaries after deformation, are converted into a *free solid-fluid macroscopic interface*, of type $\mathcal{S}^{(sf)}$ subjected to (16), with the wall boundaries remaining in contact only with the fluid phase. The combination of these two conditions is achieved by extending the standard description of contact in single-continuum problems by employing a set-valued law and a gap function [46, 47]. Accordingly, the gap function, g, is defined over the boundary surface as:

$$g = \left(\mathbf{u}^{(ext)} - \bar{\mathbf{u}}^{(s)}\right) \cdot \mathbf{n}. \tag{17}$$

In presence of closed contact conditions in $\mathbf{x} \in \partial\Omega^{(M)}$, which correspond to $g = 0$ in a

boundary point $\mathbf{x}$, the behavior of the boundary is stated by (14). Conversely, open contact in a point $\mathbf{x} \in \partial\Omega^{(M)}$ corresponds to the attainment of condition $g > 0$ in such a point, with separation of surfaces $\mathcal{S}^{(sf)}$ (where (16) applies) and $\partial\Omega^{(M)}$ (where (14) applies). In infinitesimal displacements, the undeformed and deformed configurations are superimposed. Hence, although $\mathcal{S}^{(sf)}$ and $\partial\Omega^{(M)}$ are distinct surfaces, they are superposed in a neighborhood of $\mathbf{x}$. Thus, when open contact is attained in a point $\mathbf{x} \in \partial\Omega^{(M)}$, both conditions (16) and (14) apply in such a point. Consequently, in open contact, one has simultaneously that $-p\mathbf{n} = \mathbf{t}^{(ext)}$ and $\check{\boldsymbol{\sigma}}^{(s)}\mathbf{n} = \mathbf{o}$. The first of these two relations implies that the external tractions are all transfered to the fluid phase interposing between the solid and the wall. The second relation indicates that the solid behaves as a free solid-fluid macroscopic interface. Note that this second condition is formally similar to the condition of open contact for standard unilateral contact in Cauchy single-phase continua: $\boldsymbol{\sigma}^{(s)}\mathbf{n} = \mathbf{o}$, where $\boldsymbol{\sigma}^{(s)}$ is the Cauchy stress tensor [46], although it is different since it involves the extrinsic stress tensor $\check{\boldsymbol{\sigma}}^{(s)}$.

Summary of unilateral boundary conditions for stresses

$$\begin{array}{lll} \text{closed contact:} & \check{\boldsymbol{\sigma}}^{(s)}\mathbf{n} - p\mathbf{n} = \mathbf{t}^{(ext)} & \text{if } g = \left(\mathbf{u}^{(ext)} - \bar{\mathbf{u}}^{(s)}\right)\cdot\mathbf{n} = 0 \\ \text{open contact:} & \begin{array}{rcl} -p\mathbf{n} & = & \mathbf{t}^{(ext)} \\ \check{\boldsymbol{\sigma}}^{(s)}\mathbf{n} & = & \mathbf{o} \end{array} & \text{if } g = \left(\mathbf{u}^{(ext)} - \bar{\mathbf{u}}^{(s)}\right)\cdot\mathbf{n} > 0 \end{array} \tag{18}$$

Medium-independent general stress partitioning law

Two general stress partitioning laws of medium-independent character have been derived in Part I [37].

The first one applies to regions $\Omega^{(h)}$ where the stress state is macroscopically uniform and with null relative solid-fluid motion at the boundary $\Omega^{(h)}$. By denoting $\check{\boldsymbol{\sigma}}_h^{(s)}$ and p_h the constant values of fields $\check{\boldsymbol{\sigma}}^{(s)}$ and p inside $\Omega^{(h)}$, the external traction field $\mathbf{t}^{(ext)}(\mathbf{x},\,\mathbf{n})$ over $\partial\Omega^{(h)}$, can be represented by a single constant tensor $\boldsymbol{\sigma}^{(ext)}$ associated with domain $\Omega^{(h)}$:

$$\mathbf{t}^{(ext)}(\mathbf{x},\,\mathbf{n}) = \boldsymbol{\sigma}^{(ext)}\mathbf{n}, \qquad \mathbf{x} \in \partial\Omega^{(h)} \tag{19}$$

This external stress tensor $\boldsymbol{\sigma}^{(ext)}$ is always partitioned in compliance with the following general law, irrespective of the particular constitutive and microstructural features of the medium

considered [37]:

$$\boldsymbol{\sigma}^{(ext)} = \check{\boldsymbol{\sigma}}_h^{(s)} - p_h \mathbf{I} \tag{20}$$

A second general stress partitioning law, formally similar to (20), applies to regions undergoing conditions of undrained flow. In such regions, hereby denoted as $\Omega^{(u)}$, the macroscopic relative solid-fluid motion is prevented across any surface. In this case, the traction in any point $\mathbf{x} \in \Omega^{(u)}$ over a surface of unit normal $\mathbf{n}$ turns out to be expressed as:

$$\mathbf{t}^{(ext)}(\mathbf{x},\, \mathbf{n}) = \boldsymbol{\sigma}^{(ext)}\mathbf{n}, \qquad \forall \mathbf{x} \in \Omega^{(u)},\ \ \forall \mathbf{n} \tag{21}$$

where the tensor field $\boldsymbol{\sigma}^{(ext)}$, defined over $\Omega^{(u)}$, has the expression:

$$\boldsymbol{\sigma}^{(ext)} = \check{\boldsymbol{\sigma}}^{(s)} - p\mathbf{I} \tag{22}$$

As previously observed [10, 37, 40], relations (20) and (22) coincide, from a formal point of view, with the classical tensorial statement of Terzaghi's principle upon identifying $\check{\boldsymbol{\sigma}}^{(s)}$ with the effective stress tensor.

3 Linear Isotropic formulation with volumetric-deviatoric uncoupling

This section examines the specialization of the linear formulation of the previous section under hypotheses of isotropy and volumetric-deviatoric uncoupling. In Section 3.1, as a consequence of these assumptions, suitable elastic moduli are introduced and general representations are derived of the stess-strain law of the solid phase. The corresponding linear PDE governing the response of isotropic media for negligible inertia forces are derived in Section 3.2. Finally, in Section 3.4, bounds for the elastic moduli are estimated by deploying a simple Composite Spheres Assemblage (CSA) homogenization approach [48, 49].

3.1 Linear elastic isotropic laws

As a consequence of the assumption of volumetric-deviatoric uncoupling for the solid phase and linear elastic response, the strain energy density $\bar{\psi}^{(s)}$ achieves the following quadratic form:

$$\bar{\psi}^{(s)}\left(\bar{\boldsymbol{\varepsilon}}^{(s)}_{dev},\, \bar{e}^{(s)},\, \hat{e}^{(s)}\right) = \frac{1}{2}\bar{K}^{(s)}_{dev}\left[\bar{\boldsymbol{\varepsilon}}^{(s)}_{dev}\right] : \left[\bar{\boldsymbol{\varepsilon}}^{(s)}_{dev}\right] + \frac{1}{2}\begin{bmatrix} \bar{e}^{(s)} & \hat{e}^{(s)} \end{bmatrix}\left[\bar{\boldsymbol{K}}^{(s)}_{iso}\right]\begin{bmatrix} \bar{e}^{(s)} \\ \hat{e}^{(s)} \end{bmatrix} \tag{23}$$

where the volumetric-deviatoric split is introduced for strains and energy in the usual way:

$$\bar{\boldsymbol{\varepsilon}}^{(s)} = \bar{\boldsymbol{\varepsilon}}^{(s)}_{dev} + \bar{\boldsymbol{\varepsilon}}^{(s)}_{sph}, \qquad \bar{\boldsymbol{\varepsilon}}^{(s)}_{sph} = \frac{1}{3}\mathrm{tr}\bar{\boldsymbol{\varepsilon}}^{(s)}\boldsymbol{I} = \frac{1}{3}\bar{e}^{(s)}\boldsymbol{I}, \qquad \bar{\boldsymbol{\varepsilon}}^{(s)}_{dev} = \bar{\boldsymbol{\varepsilon}}^{(s)} - \frac{1}{3}\bar{e}^{(s)}\boldsymbol{I} \tag{24}$$

$$\bar{\psi}^{(s)}\left(\bar{\boldsymbol{\varepsilon}}^{(s)},\, \hat{e}^{(s)}\right) = \bar{\psi}^{(s)}_{dev}\left(\bar{\boldsymbol{\varepsilon}}^{(s)}_{dev}\right) + \bar{\psi}^{(s)}_{sph}\left(\bar{e}^{(s)},\, \hat{e}^{(s)}\right) \tag{25}$$

Standard variationally-consistent definitions for elastic coefficientsis are considered. These are introduced as the second derivatives [40]:

$$\left[\bar{\boldsymbol{K}}^{(s)}_{iso}\right] = \begin{bmatrix} \bar{K}^{\bar{e}^{(s)}\bar{e}^{(s)}} & \bar{K}^{\hat{e}^{(s)}\bar{e}^{(s)}} \\ \bar{K}^{\hat{e}^{(s)}\bar{e}^{(s)}} & \bar{K}^{\hat{e}^{(s)}\hat{e}^{(s)}} \end{bmatrix} = \begin{bmatrix} \dfrac{\partial^2\bar{\psi}^{(s)}}{\partial\bar{e}^{(s)}\partial\bar{e}^{(s)}} & \dfrac{\partial^2\bar{\psi}^{(s)}}{\partial\hat{e}^{(s)}\partial\bar{e}^{(s)}} \\ \dfrac{\partial^2\bar{\psi}^{(s)}}{\partial\hat{e}^{(s)}\partial\bar{e}^{(s)}} & \dfrac{\partial^2\bar{\psi}^{(s)}}{\partial\hat{e}^{(s)}\partial\hat{e}^{(s)}} \end{bmatrix}, \qquad \bar{K}^{(s)}_{dev} = \frac{\partial^2\bar{\psi}^{(s)}}{\partial\left\|\bar{\boldsymbol{\varepsilon}}^{(s)}_{dev}\right\|\partial\left\|\bar{\boldsymbol{\varepsilon}}^{(s)}_{dev}\right\|}. \tag{26}$$

Owing to these definitions, the stress-strain relations for the solid phase are written as follows:

$$\check{\boldsymbol{\sigma}}^{(s)}_{dev} = \bar{K}^{(s)}_{dev}\bar{\boldsymbol{\varepsilon}}^{(s)}_{dev} \tag{27}$$

$$\begin{bmatrix} \check{p}^{(s)} \\ \hat{p}^{(s)} \end{bmatrix} = -\left[\bar{\boldsymbol{K}}^{(s)}_{iso}\right]\begin{bmatrix} \bar{e}^{(s)} \\ \hat{e}^{(s)} \end{bmatrix} \tag{28}$$

where the primary volumetric and deviatoric stresses (introduced in the standard work-association-compliant form) are:

$$\check{\boldsymbol{\sigma}}^{(s)}_{dev} = \frac{\partial\bar{\psi}^{(s)}}{\partial\bar{\boldsymbol{\varepsilon}}^{(s)}_{dev}}, \qquad \check{\boldsymbol{\sigma}}^{(s)}_{sph} = \frac{\partial\bar{\psi}^{(s)}}{\partial\bar{\boldsymbol{\varepsilon}}^{(s)}_{sph}}. \tag{29}$$

The relations involved in the volumetric-deviatoric split for stresses are the usual ones:

$$\check{\boldsymbol{\sigma}}^{(s)} = \check{\boldsymbol{\sigma}}^{(s)}_{dev} + \check{\boldsymbol{\sigma}}^{(s)}_{sph} \tag{30}$$

$$\breve{\boldsymbol{\sigma}}^{(s)}_{sph} = -\breve{p}^{(s)}\boldsymbol{I} \qquad\qquad \breve{\boldsymbol{\sigma}}^{(s)}_{dev} = \breve{\boldsymbol{\sigma}}^{(s)} + \breve{p}^{(s)}\boldsymbol{I} \tag{31}$$

In particular, the auxiliary extrinsic pressure-like scalar stress $\breve{p}^{(s)}$ is the stress quantity work associated with $-\bar{e}^{(s)}$, and, owing to (24), it is one third of the trace of the extrinsic stress tensor:

$$\breve{p}^{(s)} = -\frac{\partial\bar{\psi}^{(s)}}{\partial\bar{e}^{(s)}} = -\frac{1}{3}\mathrm{tr}\breve{\boldsymbol{\sigma}}^{(s)} \tag{32}$$

Elastic moduli

As shown in [40], a convenient representation of the solid linear elastic law can be achieved in terms of standard Lamè and bulk moduli of the *dry* porous medium (i.e., in absence of the fluid phase) when inertia forces are negligible:

$$\bar{k}_V = \bar{K}^{\bar{e}^{(s)}\bar{e}^{(s)}} - \frac{(\bar{K}^{\hat{e}^{(s)}\bar{e}^{(s)}})^2}{\bar{K}^{\hat{e}^{(s)}\hat{e}^{(s)}}}, \qquad \bar{\mu} = \frac{\bar{K}^{(s)}_{dev}}{2}, \qquad \bar{\lambda} = \bar{k}_V - \frac{2}{3}\bar{\mu} \tag{33}$$

Upon introducing the three auxiliary moduli $\hat{k}_r$, $\bar{k}_r$, and $\hat{k}_s$:

$$\hat{k}_r = \frac{\bar{K}^{\hat{e}^{(s)}\bar{e}^{(s)}}}{\bar{K}^{\hat{e}^{(s)}\hat{e}^{(s)}}}, \qquad\qquad \bar{k}_r = \phi^{(s)}\hat{k}_r = \frac{\phi^{(s)}\bar{K}^{\hat{e}^{(s)}\bar{e}^{(s)}}}{\bar{K}^{\hat{e}^{(s)}\hat{e}^{(s)}}}, \qquad \hat{k}_s = \frac{\bar{K}^{\hat{e}^{(s)}\hat{e}^{(s)}}}{\phi^{(s)}} \tag{34}$$

the stiffness matrix $\left[\bar{\boldsymbol{K}}^{(s)}_{iso}\right]$ can be expressed as:

$$\left[\bar{\boldsymbol{K}}^{(s)}_{iso}\right] = \begin{bmatrix} \bar{k}_V + \dfrac{\left(\bar{k}_r\right)^2\hat{k}_s}{\phi^{(s)}} & \bar{k}_r\hat{k}_s \\ \bar{k}_r\hat{k}_s & \hat{k}_s\phi^{(s)} \end{bmatrix} \tag{35}$$

The resulting representation for the stress-strain law is the following:

$$\breve{\boldsymbol{\sigma}}^{(s)} = 2\bar{\mu}\bar{\boldsymbol{\varepsilon}}^{(s)} + \bar{\lambda}\bar{e}^{(s)}\boldsymbol{I} - \frac{\bar{k}_r}{\phi^{(s)}}\hat{p}^{(s)}\boldsymbol{I} \tag{36}$$

$$\hat{p}^{(s)} = -\hat{k}_s\left(\bar{k}_r\bar{e}^{(s)} + \phi^{(s)}\hat{e}^{(s)}\right) \tag{37}$$

In particular, in view of relation (13), equations (36) and (37) achieve a convenient expression in terms of fluid pressure [40]:

$$\check{\boldsymbol{\sigma}}^{(s)} = 2\bar{\mu}\bar{\boldsymbol{\varepsilon}}^{(s)} + \bar{\lambda}\bar{e}^{(s)}\boldsymbol{I} - \bar{k}_r p\boldsymbol{I} \tag{38}$$

$$\frac{\phi^{(s)}}{\hat{k}_s}p = -\bar{k}_r\bar{e}^{(s)} - \phi^{(s)}\hat{e}^{(s)} \tag{39}$$

The inverse of (35) provides the compliance matrix $\left[\bar{\boldsymbol{C}}_{iso}^{(s)}\right]$:

$$\left[\bar{\boldsymbol{C}}_{iso}^{(s)}\right] = \left[\bar{\boldsymbol{K}}_{iso}^{(s)}\right]^{-1} = \begin{bmatrix} \frac{1}{\bar{k}_V} & -\frac{\bar{k}_r}{\phi^{(s)}\bar{k}_V} \\ -\frac{\bar{k}_r}{\phi^{(s)}\bar{k}_V} & \frac{1}{\phi^{(s)}}\left(\frac{1}{\hat{k}_s} + \frac{\left(\bar{k}_r\right)^2}{\phi^{(s)}\bar{k}_V}\right) \end{bmatrix} \tag{40}$$

whereby the spherical stress-strain relation reads:

$$\begin{bmatrix} \bar{e}^{(s)} \\ \hat{e}^{(s)} \end{bmatrix} = -\left[\bar{\boldsymbol{C}}_{iso}^{(s)}\right]\begin{bmatrix} \check{p}^{(s)} \\ \hat{p}^{(s)} \end{bmatrix} \tag{41}$$

Using relations (24), (27), (31), (33), (40) and (41), the inverse strain-stress law can be reconstructed:

$$\bar{\boldsymbol{\varepsilon}}^{(s)} = \bar{\boldsymbol{\varepsilon}}_{dev}^{(s)} + \frac{1}{3}\bar{e}^{(s)}\boldsymbol{I} = \frac{1}{2\bar{\mu}}\check{\boldsymbol{\sigma}}_{dev}^{(s)} + \frac{1}{3}\bar{e}^{(s)}\boldsymbol{I} = \frac{1}{2\bar{\mu}}\left(\check{\boldsymbol{\sigma}}^{(s)} + \check{p}^{(s)}\boldsymbol{I}\right) + \frac{1}{3}\bar{e}^{(s)}\boldsymbol{I} \tag{42}$$

$$\bar{\boldsymbol{\varepsilon}}^{(s)} = \frac{1+\bar{\nu}}{\bar{E}}\check{\boldsymbol{\sigma}}^{(s)} - \frac{\bar{\nu}}{\bar{E}}\mathrm{tr}\check{\boldsymbol{\sigma}}^{(s)}\,\boldsymbol{I} + \frac{\bar{k}_r}{3\phi^{(s)}\bar{k}_V}\hat{p}^{(s)}\boldsymbol{I} \tag{43}$$

$$\hat{e}^{(s)} = \frac{\bar{k}_r}{3\phi^{(s)}\bar{k}_V}\mathrm{tr}\check{\boldsymbol{\sigma}}^{(s)} - \frac{1}{\phi^{(s)}}\left(\frac{1}{\hat{k}_s} + \frac{\left(\bar{k}_r\right)^2}{\phi^{(s)}\bar{k}_V}\right)\hat{p}^{(s)} \tag{44}$$

where

$$\bar{\nu} = \frac{3\bar{k}_V - 2\bar{\mu}}{2\left(3\bar{k}_V + \bar{\mu}\right)}, \qquad \bar{E} = \frac{9\bar{k}_V\bar{\mu}}{\left(3\bar{k}_V + \bar{\mu}\right)} \tag{45}$$

Relation (43) recovers the Lamé inverse elastic laws when $\hat{p}^{(s)} = 0$. Also, for static problems, use of (10) allows expressing the relations (43) and (44) as functions of p:

$$\bar{\boldsymbol{\varepsilon}}^{(s)} = \frac{1+\bar{\nu}}{\bar{E}}\check{\boldsymbol{\sigma}}^{(s)} - \frac{\bar{\nu}}{\bar{E}}\mathrm{tr}\check{\boldsymbol{\sigma}}^{(s)}\,\boldsymbol{I} + \frac{\bar{k}_r}{3\bar{k}_V}p\boldsymbol{I} \tag{46}$$

$$\hat{e}^{(s)} = \frac{\bar{k}_r}{3\phi^{(s)}\bar{k}_V}\mathrm{tr}\check{\boldsymbol{\sigma}}^{(s)} - \left(\frac{1}{\hat{k}_s} + \frac{\left(\bar{k}_r\right)^2}{\phi^{(s)}\bar{k}_V}\right)p \tag{47}$$

For the fluid phase, the quadratic strain energy is written as:

$$\bar{\psi}^{(f)} = \phi^{(f)}\frac{1}{2}\hat{k}_f\left(\hat{e}^{(f)}\right)^2 \tag{48}$$

where $\hat{k}_f$ is the fluid intrinsic bulk modulus, whose definition is recalled below together with the fluid pressure-intrinsic strain relation:

$$\hat{k}_f = \frac{\partial^2\bar{\psi}^{(f)}}{\partial\hat{e}^{(f)}\partial\hat{e}^{(f)}}, \qquad p = -\hat{k}_f\hat{e}^{(f)}. \tag{49}$$

3.2 Governing PDE for the isotropic linear problem

Governing equations (8)-(10) are hereby specialized on account of the isotropic constitutive laws with volumetric-deviatoric uncoupling obtained in Section 2. For simplicity, henceforth, space uniformity of porosities, densities and of elastic and inertial coefficients is assumed, and external volume forces are excluded (i.e., $\bar{\mathbf{b}}^{(f,ext)} = \mathbf{o}$ and $\bar{\mathbf{b}}^{(s,ext)} = \mathbf{o}$).

3.2.1 $\bar{\mathbf{u}}^{(s)}$-$\bar{\mathbf{u}}^{(f)}$ PDE with inertial terms

The domain equations (5)-(10) are combined with the isotropic stress-strain laws (49), (27), (28) and (35), and are solved to obtain a system of equations in the primary unknowns $\bar{\mathbf{u}}^{(s)}$ and $\bar{\mathbf{u}}^{(f)}$ directly comparable with Equations (6.7) obtained by Biot in [50].

In particular, the system of (6), (49), the second of (28), and (10) can be written in the following form:

$$\begin{bmatrix} -\hat{k}_s & \hat{k}_f \\ \phi^{(s)} & \phi^{(f)} \end{bmatrix}\begin{bmatrix} \hat{e}^{(s)} \\ \hat{e}^{(f)} \end{bmatrix} = \begin{bmatrix} \frac{\bar{k}_r\hat{k}_s}{\phi^{(s)}}\bar{e}^{(s)} \\ \phi^{(s)}\bar{e}^{(s)} + \phi^{(f)}\bar{e}^{(f)} \end{bmatrix} \tag{50}$$

Hence we have:

$$\begin{aligned}\begin{bmatrix}\hat{e}^{(s)}\\ \hat{e}^{(f)}\end{bmatrix} &= -\frac{1}{\hat{k}_s\phi^{(f)}+\hat{k}_f\phi^{(s)}}\begin{bmatrix}\phi^{(f)} & -\hat{k}_f\\ -\phi^{(s)} & -\hat{k}_s\end{bmatrix}\begin{bmatrix}\frac{\bar{k}_r\hat{k}_s}{\phi^{(s)}}\bar{e}^{(s)}\\ \phi^{(s)}\bar{e}^{(s)}+\phi^{(f)}\bar{e}^{(f)}\end{bmatrix}\\ &= \begin{bmatrix}\dfrac{-\phi^{(f)}\frac{\bar{k}_r\hat{k}_s}{\phi^{(s)}}\bar{e}^{(s)}+\hat{k}_f\left(\phi^{(s)}\bar{e}^{(s)}+\phi^{(f)}\bar{e}^{(f)}\right)}{\hat{k}_s\phi^{(f)}+\hat{k}_f\phi^{(s)}}\\ \dfrac{\bar{k}_r\hat{k}_s\bar{e}^{(s)}+\hat{k}_s\left(\phi^{(s)}\bar{e}^{(s)}+\phi^{(f)}\bar{e}^{(f)}\right)}{\hat{k}_s\phi^{(f)}+\hat{k}_f\phi^{(s)}}\end{bmatrix}\end{aligned} \tag{51}$$

Substitution of (3) and (38) into (8), and substitution of (51) in (9) yield equations having a $\bar{\mathbf{u}}^{(s)}$-$\bar{\mathbf{u}}^{(f)}$ form easily comparable with equations (6.7) in [50]:

$$\begin{aligned}&\bar{\mu}\left(\nabla\cdot\nabla\right)\bar{\mathbf{u}}^{(s)}+\left(\bar{\lambda}+\bar{\mu}\right)\left(\bar{e}^{(s)}\nabla\right)+\\ &\quad+\left[\left(\phi^{(s)}+\bar{k}_r\right)^2\hat{k}_{sf}\left(\bar{e}^{(s)}\nabla\right)+\left(\phi^{(s)}+\bar{k}_r\right)\phi^{(f)}\hat{k}_{sf}\left(\bar{e}^{(f)}\nabla\right)\right]+\\ &\quad+\bar{\mathbf{b}}^{(sf)}=\bar{\rho}^{(s)}\ddot{\bar{\mathbf{u}}}^{(s)}\end{aligned} \tag{52}$$

$$\begin{aligned}&\left[\left(\phi^{(s)}+\bar{k}_r\right)\phi^{(f)}\hat{k}_{sf}\left(\bar{e}^{(s)}\nabla\right)+\left(\phi^{(f)}\right)^2\hat{k}_{sf}\left(\bar{e}^{(f)}\nabla\right)\right]+\\ &\quad-\bar{\mathbf{b}}^{(sf)}=\bar{\rho}^{(f)}\ddot{\bar{\mathbf{u}}}^{(f)}\end{aligned} \tag{53}$$

where $\hat{k}_{sf}$ is a modulus defined as:

$$\frac{1}{\hat{k}_{sf}}=\left(\frac{\phi^{(s)}}{\hat{k}_s}+\frac{\phi^{(f)}}{\hat{k}_f}\right) \tag{54}$$

and which can be interpreted as a series-coupling of solid and fluid intrinsic stiffnesses $\hat{k}_s$ and $\hat{k}_f$.

It is interesting to observe that the general structure of Biot's PDEs (6.7) is recovered, with one important difference in the particular expressions of the elastic coefficients. Actually, upon conveniently arranging the coefficients of the differential terms $\bar{e}^{(s)}\nabla$, $\bar{e}^{(f)}\nabla$, entering (52) and (53) in the matrix form:

$$\begin{bmatrix}\bar{\lambda}+\bar{\mu} & 0\\ 0 & 0\end{bmatrix}+\hat{k}_{sf}\begin{bmatrix}\left(\phi^{(s)}+\bar{k}_r\right)^2 & \left(\phi^{(s)}+\bar{k}_r\right)\phi^{(f)}\\ \left(\phi^{(s)}+\bar{k}_r\right)\phi^{(f)} & \left(\phi^{(f)}\right)^2\end{bmatrix} \tag{55}$$

these can be compared with the coefficients entering Biot's equation (6.7) which are function of

$\bar{\lambda}$, $\bar{\mu}$, and of two elastic coefficients, Q and R introduced by Biot proceeding from the synthetic consideration of a single strain energy for the whole mixture depending on both solid and fluid strains. In VMTPM, we proceed istead from the consideration of individual strain energies of the solid and fluid phases, and explicit relations are obtained for Q and R as functions of elastic coefficients of individual phases:

$$Q = \left(\phi^{(s)} + \bar{k}_r\right) \phi^{(f)} \left(\frac{\phi^{(s)}}{\hat{k}_s} + \frac{\phi^{(f)}}{\hat{k}_f}\right)^{-1}, \qquad R = \left(\phi^{(f)}\right)^2 \left(\frac{\phi^{(s)}}{\hat{k}_s} + \frac{\phi^{(f)}}{\hat{k}_f}\right)^{-1} \tag{56}$$

The important difference with Biot's equation (6.7) concerns the coefficient multiplying the term $\left(\bar{e}^{(s)}\nabla\right)$ in (52). In Biot's formulation, this is equal to $\bar{\lambda} + \bar{\mu}$. Conversely, in (52), this term turns out to be equal to:

$$\bar{\lambda} + \bar{\mu} + \left(\phi^{(s)} + \bar{k}_r\right)^2 \hat{k}_{sf} \tag{57}$$

with an *added stiffness* coupling term equal to $\left(\phi^{(s)} + \bar{k}_r\right)^2 \hat{k}_{sf}$. Also, in contrast with Biot's formulation, no *added mass* terms are present in (52) and (53).

3.3 PDE for static and quasi-static interaction

For static or quasi-static problems, the sum of (11) and (12) yields:

$$\frac{\partial \check{\sigma}_{ij}^{(s)}}{\partial x_j} - \frac{\partial p}{\partial x_i} = 0 \tag{58}$$

Substituting (3) and (38) into (58) yields:

$$\left(\bar{\mu} + \bar{\lambda}\right) (\nabla \otimes \nabla)\, \bar{\mathbf{u}}^{(s)} + \bar{\mu}\, (\nabla \cdot \nabla)\, \bar{\mathbf{u}}^{(s)} - \left(1 + \bar{k}_r\right) \nabla p = 0 \tag{59}$$

Moreover, considering the following position introducing the relative solid-fluid velocity:

$$\mathbf{w}^{(fs)} = \bar{\mathbf{u}}^{(f)} - \bar{\mathbf{u}}^{(s)} \tag{60}$$

according to which the following substitution can be performed:

$$(\nabla \otimes \nabla)\, \bar{\mathbf{u}}^{(f)} = (\nabla \otimes \nabla)\, \mathbf{w}^{(fs)} + (\nabla \otimes \nabla)\, \bar{\mathbf{u}}^{(s)}. \tag{61}$$

Upon excluding inertia terms, equation (53) provides:

$$\hat{k}_{sf}\left(\phi^{(f)}\right)^2(\nabla\otimes\nabla)\mathbf{w}^{(fs)}+\hat{k}_{sf}\phi^{(f)}\left(1+\bar{k}_r\right)(\nabla\otimes\nabla)\bar{\mathbf{u}}^{(s)}-\bar{\mathbf{b}}^{(sf)}=0 \tag{62}$$

The system of PDE (59) and (62) governing this class of quasi-static problems requires a specification of the particular solid fluid interaction. Hereby, as a simplest possible choice, a linear Darcy law is considered for $\bar{\mathbf{b}}^{(sf)}$:

$$\bar{\mathbf{b}}^{(sf)}=-\bar{\mathbf{b}}^{(fs)}=K\frac{\partial\mathbf{w}^{(fs)}}{\partial t} \tag{63}$$

where the proportionality coefficient K, in $\left[Ns/m^4\right]$, can be expressed as follows [51]:

$$K=\frac{(\phi^{(f)})^2\mu^{(f)}}{\kappa} \tag{64}$$

where $\mu^{(f)}$ is the coefficient of effective fluid viscosity, in $\left[Ns/m^2\right]$, and κ is the intrinsic permeability of the porous material, measured in $\left[m^2\right]$.

Account of (63) and of zero external volume forces in (12) provides the equation completing the system of (59) and (62):

$$\nabla p=\frac{\bar{\mathbf{b}}^{(fs)}}{\phi^{(f)}}=-\frac{K}{\phi^{(f)}}\frac{\partial\mathbf{w}^{(fs)}}{\partial t} \tag{65}$$

Inclusion of (65) into (59) and (62) yields the system of governing equations for the isotropic problem with Darcy interaction in the so-called u-w form:

$$\left(\bar{\mu}+\bar{\lambda}\right)(\nabla\otimes\nabla)\,\bar{\mathbf{u}}^{(s)}+\bar{\mu}\,(\nabla\cdot\nabla)\,\bar{\mathbf{u}}^{(s)}+\left(1+\bar{k}_r\right)\frac{K}{\phi^{(f)}}\frac{\partial\mathbf{w}^{(fs)}}{\partial t}=0 \tag{66}$$

$$\hat{k}_{sf}\left(\phi^{(f)}\right)^2(\nabla\otimes\nabla)\mathbf{w}^{(fs)}+\hat{k}_{sf}\phi^{(f)}\left(1+\bar{k}_r\right)(\nabla\otimes\nabla)\bar{\mathbf{u}}^{(s)}-K\frac{\partial\mathbf{w}^{(fs)}}{\partial t}=0 \tag{67}$$

3.4 CSA estimates of elastic moduli

Estimates of the constitutive moduli $\hat{k}_s$ and $\bar{k}_r$ have been derived in [40], based on the simple Composite Spheres Assemblage (CSA) homogenization technique established by Hashin [48,49, 52]. Derivation of CSA estimates is based on the assumption that the microstructural realization of the solid medium consists of hollow spherical cells filling out space up to the limit of zero volume of unfilled space [48, 49].

It is important to remark that the peculiarity of the CSA assumption on the microstructural realization lay aside the sought feature of medium independence for the poroelastic theory since, besides isotropy, a specific hypothesis is introduced on the realization of the microstructure of the medium. For this reason, all relations making use of these estimates will be marked as '(Obtained with CSA)'. In the following, these relations will be only prudently invoked to have subsidiary correlations between macroscopic and microscopic moduli, once microstructure-independent isotropic laws of more general validity are first obtained.

However, CSA provides relations of practical use between the macroscopic moduli $\hat{k}_s$, $\bar{k}_r$, and $\bar{k}_V$, and the elastic parameters which define the isotropic response at the microscale of the material constituting the solid phase. These parameters are the microscale shear modulus μ, the microscale bulk modulus k_s, and the microscale Poisson ratio ν, related to k_s and μ by the usual relation $\nu = (3k_s - 2\mu)/[2\,(3k_s + \mu)]$ holding for isotropic materials.

The relations provided by CSA between macroscopic and microscale elastic moduli are:

$$\bar{k}_r = -\frac{\phi^{(s)}\frac{4}{3}\mu}{\frac{4}{3}\mu + k_s(1-\phi^{(s)})}, \qquad \hat{k}_s = \frac{1}{1-\phi^{(s)}}\left[\frac{4}{3}\mu + k_s(1-\phi^{(s)})\right] \tag{68}$$

$$\bar{k}_V = \frac{\phi^{(s)}\frac{4}{3}\mu k_s}{\frac{4}{3}\mu + (1-\phi^{(s)})k_s} \tag{69}$$

An alternate equivalent expression for $\bar{k}_r$ as function of $\phi^{(s)}$ and ν is [40]:

$$\bar{k}_r = -\frac{2(1-2\nu)\phi^{(s)}}{3-3\nu-\phi^{(s)}(1+\nu)} \tag{70}$$

In view of the bounds $0 \leq \nu \leq 0.5$ and $0 \leq \phi^{(s)} \leq 1$, the following bounds apply for $\bar{k}_r$:

$$-1 \leq \bar{k}_r \leq 0 \tag{71}$$

Specifically, the upper bound 0 is achieved in the limit of vanishing solid volume fraction $\phi^{(s)} = 0$, and when the solid constituent material is volumetrically incompressible ($\nu = 0.5$); the lower bound is attained at $\phi^{(s)} = 1$.

4 Stress partitioning in ideal compression tests

Stress partitioning is hereby investigated for the cases of four ideal static infinitesimal compression tests in oedometric conditions. The macroscopic physical domain $\Omega^{(M)}$ of the boundary value problems is the mixture contained inside a cylindrical compression chamber. The boundaries of the mixture are the walls of the compression chamber and the compressive plug, see Figure 1. Cylindrical coordinates are introduced over $\Omega^{(M)}$ with x being the direction of the axis of the cylinder, and with r and θ being the radial and angular coordinates, respectively. The origin of the reference frame is set at the bottom center of the specimen of length L, directed upward along the radial axis. A compressive plug is positioned on the upper side of the specimen at $x = L$, see Figure 1. Four experimental setups are considered: a jacketed drained test (JD); an unjacketed test (U); a jacketed undrained test (JU); and a creep compression test with controlled fluid pressure and constant stress at the plug (CCFP). It should be noted that no viscous creep effects for the individual solid phase are considered in in CCFP.

For all the tests considered, isotropy and homogeneity of the initial configuration is assumed together with hypotheses of negligible gravitational forces. Accordingly, the domain equations and the boundary conditions hereby applied are those of Section 3, and the mixture is assumed to have initially uniform porosity $\phi^{(f)}$. A simple short-range solid-fluid interaction of Darcy type is also considered.

4.1 Boundary conditions

For all the tests investigated, boundary conditions on the bottom surface $\partial\Omega_b^{(M)}$ and on the lateral surface $\partial\Omega_l^{(M)}$ are the same, and correspond to unilateral contact with zero external displacement $\mathbf{u}^{(ext)}$, see (18) in Section 2. Accordingly, these surfaces are treated either as *closed contact* or as *open contact* according to the sign of $\check{\boldsymbol{\sigma}}^{(s)}\mathbf{n}\cdot\mathbf{n}$. The solution of the problem posed by this nonlinear constraint is operatively handled by initially considering trial closed contact boundary conditions. For sake of simplicity, no friction is considered, so that the external

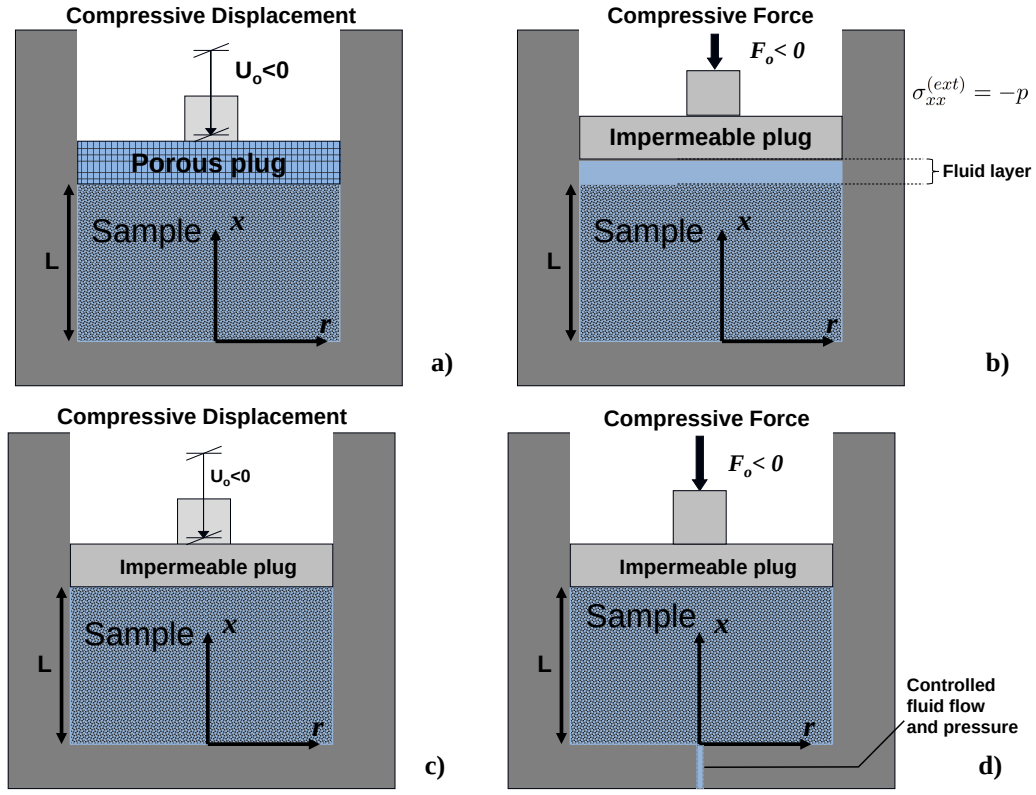

Figure 1: Schematics of the four compression tests analyzed: a) Jacketed Drained (JD) test; b) Unjacketed test (U); c) Jacketed Undrained (JU) test; d) Creep test with controlled Fluid Pressure (CCFP).

traction $\mathbf{t}^{(ext)}$ is normal to the confining walls: $\mathbf{t}^{(ext)} = \sigma_n^{(ext)}\mathbf{n}$.

On the top boundary surface $\partial\Omega_u^{(M)}$, four different ideal contact and loading conditions are considered for each of the four tests, whose descriptions are reported in the following.

Due to the quasi-static nature of the loads applied, equations (66) and (67) can be used as domain equations. Herein, the analysis is limited to the final stationary equilibrium configuration at time $t = \infty$ when consolidation phenomena have fully developed. Accordingly, time rates of $\bar{\mathbf{u}}^{(f)}$ and $\bar{\mathbf{u}}^{(s)}$ are set to zero together with the rate of $\mathbf{w}^{(fs)}$. Altogether, vanishing of $\mathbf{w}^{(fs)}$, the cylindrical symmetry of the system, and the uniformity of boundary conditions, ensure that the macroscopic displacement field of the solid, solving (66) and (67) is linear [40]. Such linearity implies that the strain and stress states inside the mixture are macroscopically homogeneous. Accordingly, the partial differential problem turns out to be conveniently converted into an algebraic one, where the unknowns are the uniform stress quantities $\check{\boldsymbol{\sigma}}_h^{(s)}$, p_h, and strains $\bar{\boldsymbol{\varepsilon}}_h^{(s)}$ and $\hat{e}^{(s)}$. Owing to space homogeneity of stresses, and in light of the medium-independent

stress partitioning laws in Section 2, a physically meaningful external stress tensor $\boldsymbol{\sigma}^{(ext)}$ can be introduced, which is related to internal stresses by the *Terzaghi-like* relation (20).

On account of the cylindrical symmetry and homogeneity of the stress field in $\Omega^{(M)}$, the stress and strain matrices in the (x, r, θ) reference system all have the transversely isotropic form:

$$\left[\breve{\boldsymbol{\sigma}}^{(s)}\right] = \begin{bmatrix} \breve{\sigma}_{xx}^{(s)} & 0 & 0 \\ 0 & \breve{\sigma}_{tt}^{(s)} & 0 \\ 0 & 0 & \breve{\sigma}_{tt}^{(s)} \end{bmatrix}, \qquad \left[\boldsymbol{\sigma}^{(ext)}\right] = \begin{bmatrix} \sigma_{xx}^{(ext)} & 0 & 0 \\ 0 & \sigma_{tt}^{(ext)} & 0 \\ 0 & 0 & \sigma_{tt}^{(ext)} \end{bmatrix} \tag{72}$$

$$\left[\bar{\boldsymbol{\varepsilon}}^{(s)}\right] = \begin{bmatrix} \bar{\varepsilon}_{xx}^{(s)} & 0 & 0 \\ 0 & \bar{\varepsilon}_{tt}^{(s)} & 0 \\ 0 & 0 & \bar{\varepsilon}_{tt}^{(s)} \end{bmatrix} \tag{73}$$

with $(\cdot)_{tt} = (\cdot)_{rr} = (\cdot)_{\theta\theta}$ being the transverse normal components of the above tensors.

The quantities that can be directly measured during the compression tests are:

- the fluid pressure inside the specimen p_h
- the external normal traction t_x^{ext} applied by the superior plate over $\partial\Omega_u^{(M)}$, and related to the force F_o measured by the load cell by:

$$t_x^{ext} = \sigma_{xx}^{(ext)} = \frac{F_o}{A} \leq 0 \quad \text{with } F_o \leq 0 \tag{74}$$

  where t_x^{ext} and $\sigma_{xx}^{(ext)}$ are equated on account of (19), and where A is the area of $\partial\Omega_u^{(M)}$, being t_x^{ext} negative for compressive tractions.

- the longitudinal strain of the specimen $\bar{\varepsilon}_x^{(ext)}$, which is the only nonzero component of the externally applied macroscopic strain $\bar{\boldsymbol{\varepsilon}}^{(ext)}$, and turns out to be related to the displacement applied at the plate U_o by:

$$\bar{\varepsilon}_x^{(ext)} = \frac{U_o}{L}, \qquad \left[\bar{\boldsymbol{\varepsilon}}^{(ext)}\right] = \begin{bmatrix} \bar{\varepsilon}_x^{(ext)} & 0 & 0 \\ 0 & 0 & 0 \\ 0 & 0 & 0 \end{bmatrix} \tag{75}$$

Taking advantage of the recognized algebraic nature of the problem at hand, the operative criterion used in the following examples to cope with unilateral contact is the following: as a trial step, bilateral undrained contact conditions (14) are first applied directly to strain components with:

$$\left[\bar{\boldsymbol{\varepsilon}}^{(s)}\right]_{trial} = \left[\bar{\boldsymbol{\varepsilon}}^{(ext)}\right] \tag{76}$$

which corresponds to setting

$$(\bar{\varepsilon}^{(s)}_{xx})_{trial} = \frac{U_o}{L} \tag{77}$$

$$(\bar{\varepsilon}^{(s)}_{tt})_{trial} = 0 \ ; \tag{78}$$

Next, a trial solution of the stress tensor $(\check{\boldsymbol{\sigma}}^{(s)})_{trial}$ is computed from $(\bar{\boldsymbol{\varepsilon}}^{(s)})_{trial}$ by applying the isotropic stress-strain relation, and the sign of $\check{\sigma}^{(s)}_{n,trial} = \check{\boldsymbol{\sigma}}^{(s)}\mathbf{n}\cdot\mathbf{n}$ is checked: if $\check{\sigma}^{(s)}_{n} > 0$, boundary conditions are switched to unilateral ones (i.e., relation (18)).

Although the response of the system is measured in terms of primary measured quantities p_h, t^{ext}_x and $\bar{\varepsilon}^{(ext)}_x$, the privileged coordinate set for tracking the volumetric mechanical state of the solid porous material is represented by the Deviatoric strain and volumetric Extrinsic and Intrinsic strain coordinates (DEI) $\bar{\boldsymbol{\varepsilon}}^{(s)}_{dev}$, $\bar{e}^{(s)}$, and $\hat{e}^{(s)}$, and by the corresponding work-associated stress and pressure coordinates ($\check{\boldsymbol{\sigma}}^{(s)}_{dev}$, $\check{p}^{(s)}$ and $\hat{p}^{(s)}$). Although measurement of DEI coordinates is not as straightforward as for the directly measurable quantities p_h, $\bar{\varepsilon}^{(s)}_{hx}$ and t^{ext}_x, such coordinate system represents, from a theoretical point of view, a basic choice within VMTPM pursuant to work-association.

When loading conditions are such that contact is preserved everywhere across the container walls, the stress path can be analyzed exclusively in terms of spherical extrinsic-intrinsic (EI) coordinates. Actually, in such a case, one has $\bar{\boldsymbol{\varepsilon}}^{(s)} = \bar{\boldsymbol{\varepsilon}}^{(ext)}$, and by virtue of volumetric-deviatoric uncoupling (27)-(28) and of the *Terzaghi-like* variational partitioning law for homogeneous stresses relation (20), the following relations hold:

$$\bar{\boldsymbol{\varepsilon}}^{(s)}_{dev} = \bar{\boldsymbol{\varepsilon}}^{(ext)}_{dev}, \qquad \left[\boldsymbol{\sigma}^{(ext)}_{dev}\right] = \left[\check{\boldsymbol{\sigma}}^{(s)}_{dev}\right] = \bar{K}^{(s)}_{dev}\begin{bmatrix} \frac{2}{3}\bar{\varepsilon}^{(ext)}_x & 0 & 0 \\ 0 & -\frac{1}{3}\bar{\varepsilon}^{(ext)}_x & 0 \\ 0 & 0 & -\frac{1}{3}\bar{\varepsilon}^{(ext)}_x \end{bmatrix} \tag{79}$$

Thus, the deviatoric part of stresses is immediately related to the external applied strain by (75). For this reason, for each of the four tests examined, the response of the porous medium will be analyzed in terms of both primary measurable quantities and EI coordinates, postponing a separate evaluation of deviatoric stresses only in case of violation of closed-contact conditions.

For what concerns spherical coordinates, an external pressure p^{ext} can be standardly defined on account of the cylindrical symmetry by taking one third of the trace of (20):

$$p^{ext} = \check{p}_h^{(s)} + p_h \tag{80}$$

with

$$p^{ext} = -\frac{1}{3}\mathrm{tr}\,\boldsymbol{\sigma}^{(ext)} = -\frac{1}{3}\left(\sigma_{xx}^{(ext)} + 2\sigma_{tt}^{(ext)}\right) \tag{81}$$

The extrinsic and intrinsic constitutive laws for the solid phase provided by (36) and (37) are respectively written:

$$\check{\boldsymbol{\sigma}}_h^{(s)} = 2\bar{\mu}\bar{\boldsymbol{\varepsilon}}_h^{(s)} + \bar{\lambda}\bar{e}_h^{(s)}\boldsymbol{I} - \bar{k}_r p_h \boldsymbol{I} \tag{82}$$

$$\frac{\phi^{(s)}}{\hat{k}_s} p_h = -\bar{k}_r \bar{e}_h^{(s)} - \phi^{(s)}\hat{e}_h^{(s)} \tag{83}$$

By taking one third of the trace of (82), one obtains:

$$\check{p}_h^{(s)} = -\bar{k}_V \bar{e}_h^{(s)} + \bar{k}_r p_h \tag{84}$$

When closed contact is preserved at the boundaries, it is inferred from (76) that $\bar{e}_h^{(s)}$ is also directly observable, being $\bar{e}_h^{(s)} = \bar{\varepsilon}_x^{(ext)}$. Since the strain applied by the impermeable plate ($\bar{e}_h^{(s)}$) and the fluid pressure (p_h) are quantities that can be measured more easily than the extrinsic solid pressure ($\check{p}_h^{(s)}$), it is convenient to recast the previous equations in a form conveniently involving only the directly observable quantities p^{ext}, p_h, and $\bar{e}_h^{(s)}$. Accordingly, equation (80) can be solved for p_h and substituted into (84). This yields:

$$p^{ext} = -\bar{k}_V \bar{e}_h^{(s)} + \left(1 + \bar{k}_r\right) p_h \tag{85}$$

Notably, relation (85) is in full agreement with the well known p^{ext}-$\bar{e}^{(s)}$-p relations obtained by experimental measures on sandstone [21]. In such contribution, Nur and Byerlee have experimentally investigated the optimality of several strain-pressure relations of the form:

$$p^{ext} = -\bar{k}_V \bar{e}_h^{(s)} + \alpha p_h \tag{86}$$

where α is a fitting coefficient generally referred to as the *Biot's coefficient* [53]. Validated by direct measurements of p^{ext}, $\bar{e}^{(s)}$ and p on sandstone specimens, the best fitting expression for α is reported in [21]: $\alpha = 1 - \bar{k}_V/k_s$. The combination of this expression with (86) (which corresponds to the combination of equations (3), (4), (6) and (7) in [21]) hence turns out to be equal to

$$p^{ext} = -\bar{k}_V \bar{e}_h^{(s)} + \left(1 - \frac{\bar{k}_V}{k_s}\right) p_h. \tag{87}$$

On the other hand, relation (87), which is of experimental origin in [21], turns out to be the result of a pure theoretical deduction in VMTPM. Actually, it is noteworthy exactly the one inferred from (85) when minimal CSA homogenization estimates are exploited to relate $\bar{k}_r$ to the microscale solid bulk modulus k_s. As a matter of fact, (68) and (69) yield:

$$1 + \bar{k}_r = 1 - \frac{\bar{k}_V}{k_s} \qquad \text{(Obtained with CSA)} \tag{88}$$

which substituted in (85) provides (87). Hence, for CSA-microstructured media, such an identification also yields that $\bar{k}_r$ is related to Biot's coefficient by $\bar{k}_r = \alpha - 1$.

4.2 Ideal jacketed drained test

In a jacketed drained test, compression occurs via a porous plate allowing for fluid exchange between the specimen and the environment, see Figure 1a. Hence, when mechanical equilibrium is reached, the fluid pressure in the sample is null ($p = 0$). Accordingly, the equation (36) recovers the Navier law for a single continuum. Moreover, upon considering closed contact and accounting for relation (74), compressive (negative) normal stress is recognized to exist on the whole $\partial\Omega^{(M)}$:

$$\check{\sigma}_{xx}^{(s)} < 0, \qquad \check{\sigma}_{yy}^{(s)} = \check{\sigma}_{zz}^{(s)} = \frac{\bar{\lambda}}{2\bar{\mu} + \bar{\lambda}} \check{\sigma}_{xx}^{(s)} < 0 \tag{89}$$

The condition of closed contact is thus confirmed to hold everywhere in $\partial\Omega^{(M)}$, so that the stress states can be simply analyzed in EI coordinates, being the deviatoric stress $\boldsymbol{\sigma}_{dev}^{(ext)}$ related to $\bar{\varepsilon}_x^{(ext)}$ by (79). Hence, relation (85) recovers the following expression as a special condition:

$$p^{ext} = -\bar{k}_V \bar{e}^{(s)} \tag{90}$$

and (13) provides:

$$\hat{p}^{(s)} = 0 \tag{91}$$

so that the stress path in the plane of normal spherical coordinates ($\hat{p}^{(s)}$, $\check{p}^{(s)}$) is a horizontal straight line, see Figure 2a. The inclination of the volumetric strain paths shown in Figure 2b is inferred from equation (37) considering zero fluid pressure:

$$\frac{\hat{e}^{(s)}}{\bar{e}^{(s)}} = -\frac{\bar{k}_r}{\phi^{(s)}} \tag{92}$$

The CSA estimates (68) and (70) provide expressions for $\bar{k}_r$ in terms of $\phi^{(s)}$, μ and k_s, and in terms of $\phi^{(s)}$ and ν, respectively. Accordingly, the strain ratio reads:

$$\frac{\hat{e}^{(s)}}{\bar{e}^{(s)}} = \frac{\frac{4}{3}\mu}{\frac{4}{3}\mu + k_s(1-\phi^{(s)})} = \frac{2(1-2\nu)}{3-3\nu-\phi^{(s)}(1+\nu)} \qquad \text{(Obtained with CSA)} \tag{93}$$

Note that in the Limit of Vanishing Porosity (LVP) (i.e., $\phi^{(s)} = 0$), expression (93) achieves a unit value. Hence, the slope of the strain vector in Figure 2 is $1:1$. Also, in the Limit of Incompressible Constituent Material (LICM) (i.e., $\nu = 0.5$), the ratio is zero.

4.3 Ideal unjacketed test

In the unjacketed test, the compressing plug is impermeable, and the chamber is fully occupied by the specimen and the fluid, see Figure 1b. The space between the plug and the specimen is occupied by the fluid phase: there is no direct contact between the plug and the upper boundary $\partial\Omega_u^{(M)}$. Under these mechanical conditions, the plug induces a stress state directly over the fluid phase which, in its turn, compresses the porous specimen. Accordingly, $\partial\Omega_u^{(M)}$ is a free

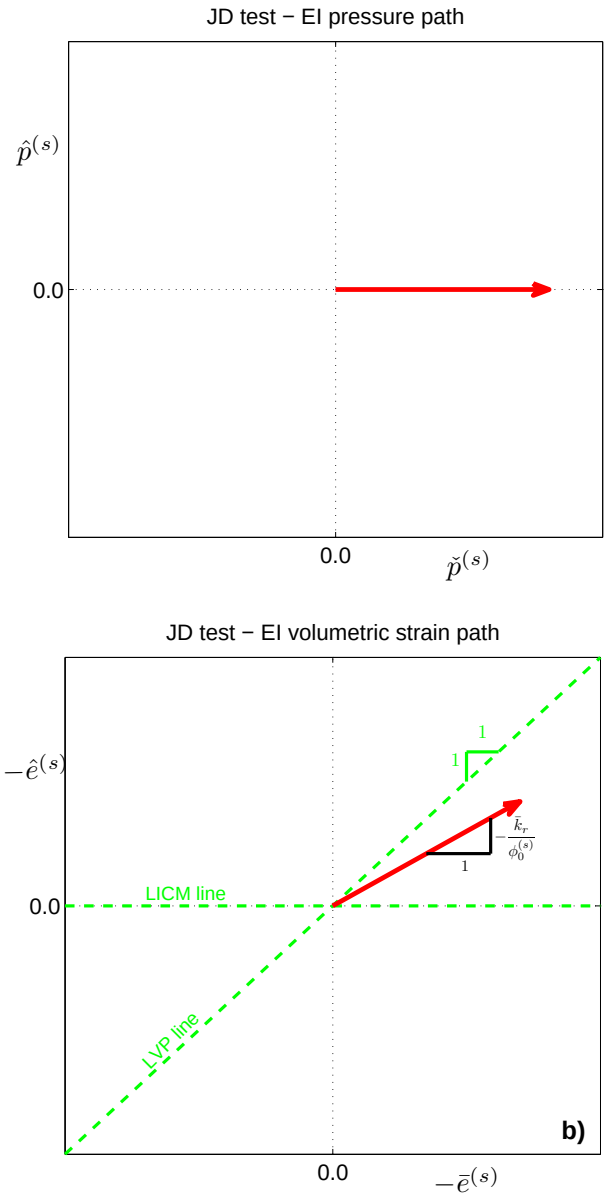

Figure 2: Representation in EI coordinates of the volumetric mechanical response during a Jacketed drained test. a) EI pressure path in the ($\hat{p}^{(s)}$, $\check{p}^{(s)}$) plane; b) EI volumetric strain path in the ($\bar{e}^{(s)}$, $\hat{e}^{(s)}$) plane. Dotted lines indicate the LVP and LICM limits.

solid-fluid macroscopic interface of type $\mathcal{S}^{(sf)}$, where the surface condition (16) applies:

$$\check{\sigma}_{xx}^{(s)} = 0, \qquad \text{over } \partial\Omega_u^{(M)} \tag{94}$$

On the upper boundary of $\Omega^{(M)}$, equilibrium between the plug and the fluid is expressed

considering a null extrinsic stress tensor in (14):

$$\sigma_{xx}^{(ext)} = -p \tag{95}$$

Hence, relations (94) and (95) correspond, from a practical point of view, to an open contact condition over $\partial\Omega_u^{(M)}$, and p can be regarded as the stress input for the specimen.

Response under bilateral contact

For the boundary $\partial\Omega_l^{(M)}$, if bilateral contact conditions are considered, we have:

$$\bar{\varepsilon}_{tt}^{(s)} = 0 \tag{96}$$

Hence, specialization of the equation (36) for the xx component yields:

$$\left(2\bar{\mu} + \bar{\lambda}\right) \bar{\varepsilon}_{xx}^{(s)} - \bar{k}_r p \;\; = \;\; 0 \tag{97}$$

It follows that:

$$\bar{e}^{(s)} = \bar{\varepsilon}_{xx}^{(s)} = \frac{\bar{k}_r}{2\bar{\mu} + \bar{\lambda}} p < 0 \tag{98}$$

Given the above relations, the transverse normal stress component reads:

$$\check{\sigma}_{tt}^{(s)} = -\bar{k}_r \frac{2\bar{\mu}}{2\bar{\mu} + \bar{\lambda}} p > 0 \tag{99}$$

The positive sign of $\check{\sigma}_{tt}^{(s)}$ indicates that, when bilateral contact is ensured, VMTPM predicts that a tensile increment of extrinsic stress (or, in presence of prestress, a decrease of compressive extrinsic stress) can be even induced as the effect of external compressive loadings. This prediction of the onset of tensile extrinsic stress increments in response to compressive loading is peculiar of VMTPM, as previously pointed out [40].

Moreover, since (98) and (39) yield:

$$\hat{e}^{(s)} = -\left(\frac{\bar{k}_r^2}{\phi^{(s)} \left(2\bar{\mu} + \bar{\lambda}\right)} + \frac{1}{k_s} \right) \tag{100}$$

from (2), the variation of solid volume fraction $d\phi^{(s)}$ turns out to be:

$$d\phi^{(s)} = -\phi^{(s)} \left[\frac{1}{k_s} + \frac{\bar{k}_r}{2\bar{\mu} + \bar{\lambda}} \left(\frac{\bar{k}_r}{\phi^{(s)}} + 1 \right) \right] \tag{101}$$

which can be negative depending on the relative values of the elastic moduli inside the square brackets.

Both the insurgence of positive increments of extrinsic normal stresses, shown by (99), and the possibility of negative $d\phi^{(s)}$ are particularly significant in cohesionless mixtures. In these materials where friction plays a primary role in the overall stability, these features can be respectively put in direct relation with decrease of confining (effective) stress and with the (relative) increment of intergranular space $d\phi^{(f)} = -d\phi^{(s)} > 0$. Such two features determine a decrease in friction which can be put in relation with the insurgence of phenomena of liquefaction occurring in low density saturated soils [54,55]. In this respect, it is important to remark that, although liquefaction is mostly known to be associated with laboratory and in situ conditions as an effect essentially induced by deviatoric undrained loading and excitations, there exist experimental evidences indicating that sands can be also liquefied by isotropic compressive stress applied under quasistatic drained conditions [56].

Response under unilateral contact

When the closed contact condition is violated according to (18), open contact has to be considered also on $\partial\Omega_l^{(M)}$. Consequently, open contact conditions $(18)_2$ apply across the whole $\partial\Omega^{(M)}$:

$$\check{\boldsymbol{\sigma}}^{(s)}\mathbf{n} = \mathbf{o}, \qquad \text{over } \partial\Omega^{(M)} \tag{102}$$

As a result, recalling that $\check{\boldsymbol{\sigma}}^{(s)}$ is uniform, one infers $\check{\boldsymbol{\sigma}}^{(s)} = \mathbf{O}$. Accordingly, one has:

$$\check{p}^{(s)} = 0 \tag{103}$$

In this case, due to (103), the normalized spherical stress path is a vertical line, as shown in Figure 3a.

It is important to remark that, when contact is lost, (79) no longer holds since, due to equations (46) and (24), one has $\bar{\boldsymbol{\varepsilon}}_{dev}^{(s)} = \mathbf{O}$ and hence $\bar{\boldsymbol{\varepsilon}}_{dev}^{(s)} \neq \bar{\boldsymbol{\varepsilon}}_{dev}^{(ext)}$.

The configuration of the unjacketed compression test is characterized via (84) in terms of

primary measured quantities by the following condition:

$$-\bar{k}_V \bar{e}^{(s)} + \bar{k}_r p = 0 \tag{104}$$

which yields:

$$p = \frac{\bar{k}_V}{\bar{k}_r} \bar{e}^{(s)} \tag{105}$$

Substituting (105) into (37), the intrinsic-to-extrinsic strain ratio for the U test is:

$$\frac{\hat{e}^{(s)}}{\bar{e}^{(s)}} = -\left(\frac{1}{\hat{k}_s} \frac{\bar{k}_V}{\bar{k}_r} + \frac{\bar{k}_r}{\phi^{(s)}} \right) \tag{106}$$

For a medium with a CSA microstructure, using (68) and (69), the special form achieved by (106) is:

$$\frac{\hat{e}^{(s)}}{\bar{e}^{(s)}} = 1 \qquad \text{(Obtained with CSA)} \tag{107}$$

Also, for such a medium, the stiffness coefficient in (105) coincides with the microscale solid bulk modulus:

$$-\bar{e}^{(s)} = \frac{1}{k_s} p \qquad \text{(Obtained with CSA)} \tag{108}$$

since (68) and (69) yield:

$$-\frac{\bar{k}_r}{\bar{k}_V} = \frac{1}{k_s} \qquad \text{(Obtained with CSA)} \tag{109}$$

4.4 Ideal jacketed undrained test

Stress partitioning in the jacketed undrained (JU) test has been previously described [40]. Hereby, the stress partitioning solution is recalled and expanded with considerations on the consequences of unilateral contact, and analyzed in terms of volumetric strain and stress EI paths. An impermeable plug compresses the sample by displacing of U_0 (< 0), see Figure 1c.

Response under bilateral contact

The trial condition of bilateral contact along the whole $\partial\Omega^{(M)}$ is initially considered. Accordingly, as a first step, the trial boundary conditions expressed by the first of (18) are applied.

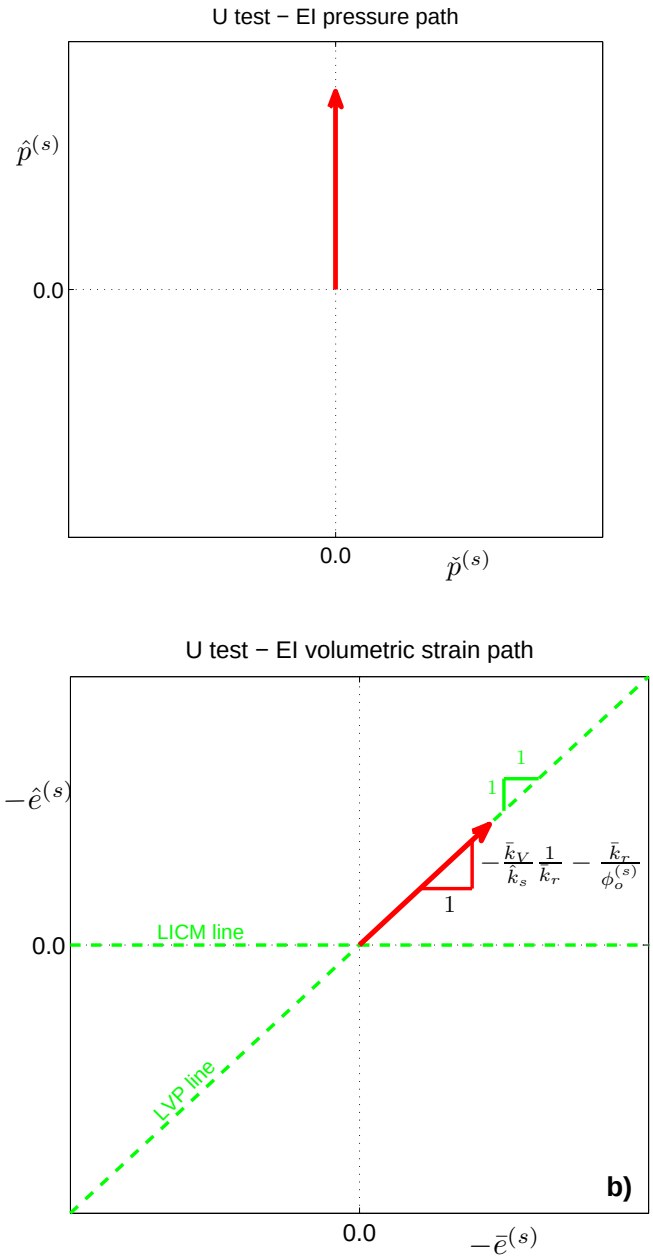

Figure 3: Representation in EI coordinates of the volumetric mechanical response during an ideal unjacketed compression test. a) EI pressure path in the $(\hat{p}^{(s)}, \check{p}^{(s)})$ plane; b) EI volumetric strain path in the $(\bar{e}^{(s)}, \hat{e}^{(s)})$ plane. Dotted lines indicate the LVP and LICM limits.

In particular, these conditions for displacements and stresses over $\partial\Omega_u^{(M)}$ are respectively:

$$\bar{u}_x^{(s)} = \bar{u}_x^{(f)} = U_0 \tag{110}$$

$$\sigma_{xx}^{(ext)} = \breve{\sigma}_{xx}^{(s)} - p \tag{111}$$

As shown in [40], strains in the mixture for a jacketed undrained test with closed contact at the boundaries are such that:

$$\bar{e}^{(f)} = \bar{e}^{(s)} \tag{112}$$

with $\bar{e}^{(s)} = \bar{\varepsilon}_{xx}^{(s)} = \frac{U_o}{L}$ in the cylindrical configuration. Denoting by $\mathbf{i}$ the unit vector of the x axis and by $(\mathbf{i} \otimes \mathbf{i})$ the associated projector, the corresponding *trial* stress solution to the system composed of (6), (38), (39) and (112) is:

$$p = -\left(1 + \bar{k}_r\right) \hat{k}_{sf} \frac{U_o}{L} \tag{113}$$

$$\breve{\boldsymbol{\sigma}}^{(s)} = 2\bar{\mu} \frac{U_o}{L} (\mathbf{i} \otimes \mathbf{i}) + \left[\bar{\lambda} + \hat{k}_{sf} \bar{k}_r \left(1 + \bar{k}_r\right)\right] \frac{U_o}{L} \boldsymbol{I} \tag{114}$$

$$\hat{p}^{(s)} = -\phi^{(s)} \left(1 + \bar{k}_r\right) \hat{k}_{sf} \frac{U_o}{L} \tag{115}$$

By computing from (114) the trial longitudinal and transverse extrinsic normal tractions $\breve{\sigma}_{xx}^{(s)}$ and $\breve{\sigma}_{tt}^{(s)}$, one has:

$$\breve{\sigma}_{xx}^{(s)} = \left[2\bar{\mu} + \bar{\lambda} + \hat{k}_{sf} \bar{k}_r \left(1 + \bar{k}_r\right)\right] \frac{U_o}{L} \tag{116}$$

$$\breve{\sigma}_{tt}^{(s)} = \left[\bar{\lambda} + \hat{k}_{sf} \bar{k}_r \left(1 + \bar{k}_r\right)\right] \frac{U_o}{L} \tag{117}$$

For bilateral boundary conditions, and when $\breve{\sigma}_{xx}^{(s)} < \breve{\sigma}_{tt}^{(s)} < 0$, closed contact is preserved all through $\partial\Omega^{(M)}$. In this last case, the true stress state in the mixture is defined by (113)-(115). The corresponding expression of Skempton's coefficient B [57], defined as the ratio of the induced fluid pressure p to the applied stress t_x^{ext}, has been computed in [40]:

$$B = \frac{p}{\sigma_{xx}^{(ext)}} = -\frac{\left(1 + \bar{k}_r\right) \hat{k}_{sf}}{2\bar{\mu} + \bar{\lambda} + \left(1 + \bar{k}_r\right)^2 \hat{k}_{sf}} \tag{118}$$

A similar coefficient B_{iso} can be defined in terms of pressure ratio as:

$$B_{iso} = \frac{p}{p^{ext}} = \frac{\left(1 + \bar{k}_r\right) \hat{k}_{sf}}{\frac{2}{3}\bar{\mu} + \bar{\lambda} + \left(1 + \bar{k}_r\right)^2 \hat{k}_{sf}} \tag{119}$$

The intrinsic-to-extrinsic pressure ratio can then be computed by recalling (13), (80), and (111):

$$\frac{\hat{p}^{(s)}}{\check{p}^{(s)}} = \phi^{(s)} \frac{B_{iso}}{1 - B_{iso}} = \frac{\phi^{(s)} \left(1 + \bar{k}_r\right) \hat{k}_{sf}}{\frac{2}{3}\bar{\mu} + \bar{\lambda} + \bar{k}_r \left(1 + \bar{k}_r\right) \hat{k}_{sf}} \tag{120}$$

For non-liquefying mixtures, the volumetric strain ratio is obtained substituting (115) and $\bar{e}^{(s)} = \frac{U_o}{L}$ into (37):

$$\frac{\hat{e}^{(s)}}{\bar{e}^{(s)}} = \frac{\left(1 + \bar{k}_r\right) \hat{k}_{sf}}{\hat{k}_s} - \frac{\bar{k}_r}{\phi^{(s)}} \tag{121}$$

Figure 4 illustrates the volumetric stress and strain paths for the JU test with unilateral contact.

Unilateral boundary conditions

The positivity of $\check{\sigma}_{xx}^{(s)}$ and $\check{\sigma}_{tt}^{(s)}$ determined by (116) is now studied to check the effective closed/open contact conditions (18). Since $U_o < 0$, open contact corresponds to the negativity of the expressions under square brackets in such relations. Also, recalling that $\bar{k}_r$ is negative, when $\bar{\mu}$ and $\bar{\lambda}$ are small compared to $\hat{k}_{sf}$, then $\check{\sigma}_{xx}^{(s)}$ and $\check{\sigma}_{tt}^{(s)}$ can attain positive values (i.e. tensile) even in presence of compressive loads. Since one trivially has:

$$2\bar{\mu} + \bar{\lambda} + \hat{k}_{sf}\bar{k}_r \left(1 + \bar{k}_r\right) > \bar{\lambda} + \hat{k}_{sf}\bar{k}_r \left(1 + \bar{k}_r\right) \tag{122}$$

a strong and a weaker condition of contact loss can be recognized, depending on the specific values of the elastic moduli $\bar{\mu}$, $\bar{\lambda}$, $\bar{k}_r$, $\hat{k}_s$, and $\hat{k}_f$ of a given isotropic mixture.

Specifically, when the stronger condition holds:

$$2\bar{\mu} + \bar{\lambda} + \hat{k}_{sf}\bar{k}_r \left(1 + \bar{k}_r\right) < 0 \tag{123}$$

then $\check{\sigma}_{tt}^{(s)} > \check{\sigma}_{xx}^{(s)} > 0$. This corresponds to the insurgence of open contact all throughout the boundary in response to compression by the plug, with $\check{\boldsymbol{\sigma}}^{(s)}\mathbf{n} = \mathbf{o}$ everywhere on $\partial\Omega^{(M)}$. These boundary conditions coincide exactly with those in (102) of Section 4.3. It is thus recognized that, when condition (123) is fulfilled, the response of the system corresponds to the same of the unjacketed test. On the other hand, when (123) does not apply but the weaker condition holds:

$$\bar{\lambda} + \hat{k}_{sf}\bar{k}_r \left(1 + \bar{k}_r\right) < 0 \tag{124}$$

then $\breve{\sigma}_{tt}^{(s)} > 0 > \breve{\sigma}_{xx}^{(s)}$ and, in response to plug compression, contact opens only on the lateral boundary.

It is worth recalling that, in case of contact loss, the relation $\boldsymbol{\sigma}_{dev}^{(ext)} = \breve{\boldsymbol{\sigma}}_{dev}^{(s)}$ remains true (since the fluid is incapable of carrying any deviatoric stress). However insurgence of open contact determines $\bar{\boldsymbol{\varepsilon}}_{dev}^{(s)} \neq \bar{\boldsymbol{\varepsilon}}_{dev}^{(ext)}$, so that all relations in (79) no longer apply, as previously observed.

Cohesionless granular materials

For cohesionless media, conditions (123) and (124) achieve an even stronger mechanical significance. Actually, in such materials, vanishing of extrinsic stress determines vanishing of intergranular (effective) stress. Consequently the loss of frictional interaction produced by opening contact is not limited to $\partial\Omega^{(M)}$, but it affects all surfaces interior to the specimen. On these surfaces, condition $\breve{\boldsymbol{\sigma}}^{(s)}\mathbf{n} = \mathbf{o}$ applies with $\mathbf{n}$ being the normal to the interior surface. As a consequence, friction is prevented across these internal surfaces, and this determines potential sliding in a way similar to liquids. Hence, conditions (123) and (124) discriminate the proneness of a given cohesionless mixture to liquefaction. For this reason we define a cohesionless mixture to be *full liquefying* when its elastic moduli are such that the stronger condition (123) holds, and to be *partially liquefying cohesionless mixture* when only the weaker condition (124) is verified. When neither condition is verified, the cohesionless medium is denominated a *non-liquefying cohesionless mixture*. In particular, condition (123) is expected to be attained for mixtures such as water-saturated loose sands. In such mixtures, the moduli $\hat{k}_s$ and $\hat{k}_f$ are expected to have magnitude much higher than the macroscopic aggregate modulus $2\bar{\mu}+\bar{\lambda}$. Hence, $\hat{k}_{sf} >> 2\bar{\mu}+\bar{\lambda}$ and, when $\bar{k}_r$ retains a nonvanishing value, the second negative term in (123) prevails over the first one.

For fully liquefying mixtures, even in the JU test, primary measured quantities comply with the unjacketed relation (104), and $\frac{\hat{e}^{(s)}}{\bar{e}^{(s)}}$ recover the other corresponding unjacketed relations also reported in Section 4.3.

Media with CSA microstructure

All previously reported relations hold for generic isotropic media, since no assumptions for their specific microstructural realization has been made. Special expressions, holding for media with CSA microstructure, can be obtained substituting relations (68), (69), and (54) in (120) and

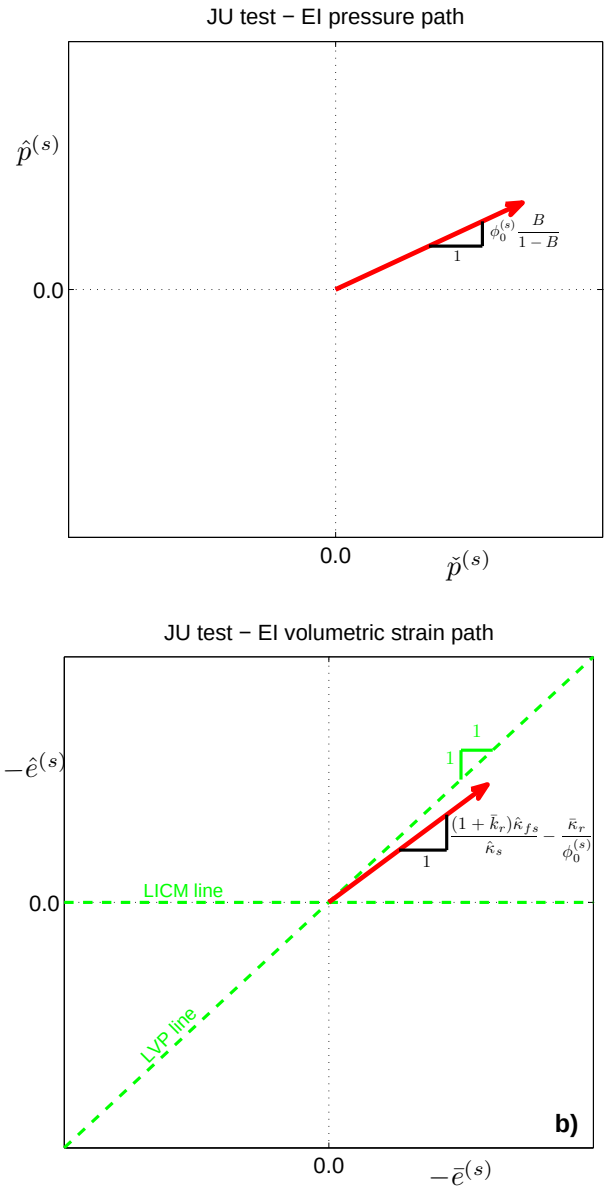

Figure 4: Representation in EI coordinates of the volumetric mechanical response during an ideal jacketed undrained compression test. a) EI pressure path in the $(\hat{p}^{(s)}, \check{p}^{(s)})$ plane; b) EI volumetric strain path in the $(\bar{e}^{(s)}, \hat{e}^{(s)})$ plane. Dotted lines indicate the LVP and LICM limits.

(121), and considering that, for the fluid phase, the macro- and microscale bulk moduli $\hat{k}_f$ and k_f coincide:

$$\frac{\hat{p}^{(s)}}{\check{p}^{(s)}} = \frac{k_f\left(\frac{4}{3}\mu + k_s\right)}{\mu\left(k_s - k_f\right)} \qquad \text{(Obtained with CSA)} \tag{125}$$

$$\frac{\hat{e}^{(s)}}{\bar{e}^{(s)}} = \frac{\frac{4}{3}\mu + k_f}{\frac{4}{3}\mu + \phi^{(s)}k_f + (1-\phi^{(s)})k_s} \qquad \text{(Obtained with CSA)} \tag{126}$$

Although the relations (125) and (126) are less general, they allow examining some limit behaviors of the system in relation to the microscale fluid stiffness. In particular, when the fluid stiffness is zero, the JD response is recovered. When the microscale bulk stiffnesses of the two materials coincide (i.e., when $k_s = k_f$), the stress and strain ratios recover the response characteristic of the unjacketed compression test. Also, at LVP (i.e., when $\phi^{(s)} \simeq 1$), the strain ratio achieves unity as expected. This implies that, when porosity is low, the volumetric strain path stays in close proximity of the LVP line.

4.5 Creep test with controlled pressure

In the CCFP test, an external pressure p_0^{ext} is kept constant via an impermeable plug. The fluid pressure in the biphasic medium is quasi-statically decreased by controlling the fluid outflow through a valve until reaching equilibrium (i.e., zero fluid pressure), see Figure 1d. The stress path in volumetric coordinates is shown in Figure 5, and it is composed of two stages: the first one consists of an unjacketed path up to $p_0 = p_0^{ext}$, and ends up with a stress state in the solid defined as $\check{\boldsymbol{\sigma}}_0 = \mathbf{O}$ and $\hat{p}_0^{(s)} = \phi^{(s)}p_0$; the second stage is determined by quasi-statically decreasing p from p_0 to 0 (allowing for controlled fluid exudation), while keeping constant the external pressure p_0^{ext}.

In the transition between the first and the second stage, closed contact conditions between the plug and $\partial\Omega_u^{(M)}$ are restored with unaltered stress state in the mixture (i.e., $\check{\boldsymbol{\sigma}} = \mathbf{O}$, $\hat{p}_0^{(s)} = \phi^{(s)}p_0$, and $p = p_0$). This condition ensures that no fluid is interposed between the specimen and the compressive plug. During the second stage, the volumetric stress components read (see relations (80) and (13)):

$$p_0^{ext} = \check{p}^{(s)} + p, \qquad \hat{p}^{(s)} = \phi^{(s)}p = \phi^{(s)}\left(p_0^{ext} - \check{p}^{(s)}\right) \tag{127}$$

Differentiating relation (127), the relevant increments read:

$$d\check{p}^{(s)} = -dp, \qquad d\hat{p}^{(s)} = \phi^{(s)}dp \tag{128}$$

The sign of the extrinsic stress increments $\check{\sigma}_{xx}^{(s)}$ and $\check{\sigma}_{tt}^{(s)}$ are evaluated to check the open/closed contact conditions. During the second loading stage, pressure reduces and strain variations are related by (84):

$$d\check{p}^{(s)} = -\bar{k}_V d\bar{e}^{(s)} + \bar{k}_r dp \tag{129}$$

and, accounting for $(128)_1$, one infers:

$$dp = \frac{\bar{k}_V}{(1+\bar{k}_r)} d\bar{e}^{(s)} \tag{130}$$

having both $dp < 0$ and $d\bar{e}^{(s)} < 0$. Due to the zero condition for $\check{\boldsymbol{\sigma}}_0^{(s)}$, the extrinsic stress increments $d\check{\sigma}_{xx}^{(s)}$ coincide with their overall value, viz.:

$$\check{\sigma}_{xx}^{(s)} = \check{\sigma}_{0xx}^{(s)} + d\check{\sigma}_{xx}^{(s)} = d\check{\sigma}_{xx}^{(s)} \tag{131}$$

Similarly, we have $d\check{\sigma}_{tt}^{(s)} = \check{\sigma}_{tt}^{(s)}$. Variations of trial normal stresses can then be computed applying (36) to strain and stress increments accounting for the property $d\bar{\varepsilon}_{xx}^{(s)} = d\bar{e}^{(s)}$:

$$d\check{\sigma}_{xx}^{(s)} = \left(2\bar{\mu} + \bar{\lambda}\right) d\bar{e}^{(s)} - \bar{k}_r dp, \qquad d\check{\sigma}_{tt}^{(s)} = \bar{\lambda} d\bar{e}^{(s)} - \bar{k}_r dp \tag{132}$$

Moreover, in consideration of relation (130), one has:

$$d\check{\sigma}_{xx}^{(s)} = \left(2\bar{\mu} + \bar{\lambda} - \frac{\bar{k}_r \bar{k}_V}{(1+\bar{k}_r)}\right) d\bar{e}^{(s)}, \qquad d\check{\sigma}_{tt}^{(s)} = \left(\bar{\lambda} - \frac{\bar{k}_r \bar{k}_V}{(1+\bar{k}_r)}\right) d\bar{e}^{(s)} \tag{133}$$

Since $d\bar{e}^{(s)}$ is negative and the terms in round brackets are positive, it is recognized that closed contact conditions are never violated during the CCFP test. Hence, an account of linear bilateral boundary constraint is sufficient for the analysis of this test.

The ratio $\frac{d\hat{e}^{(s)}}{d\bar{e}^{(s)}}$ is similarly computed by substituting (130) into (37), upon writing the latter for strain and stress increments:

$$\frac{\phi^{(s)}}{\hat{k}_s} dp = -\bar{k}_r d\bar{e}^{(s)} - \phi^{(s)} d\hat{e}^{(s)} \tag{134}$$

Substitution yields:

$$\frac{d\hat{e}^{(s)}}{d\bar{e}^{(s)}} = -\left(\frac{1}{\hat{k}_s}\frac{\bar{k}_V}{(1+\bar{k}_r)} + \frac{\bar{k}_r}{\phi^{(s)}}\right) \tag{135}$$

Media with CSA microstructure

The CSA estimates for relation (135) yield:

$$\frac{d\hat{e}^{(s)}}{d\bar{e}^{(s)}} = \frac{\frac{4}{3}\bar{\mu}}{\frac{4}{3}\bar{\mu}+k_s} = \frac{2\,(1-2\nu)}{3\,(1-\nu)} \qquad \text{(Obtained with CSA)} \tag{136}$$

This ratio is always positive, so that the corresponding vector in the EI volumetric strain space has a positive slope, albeit bounded by the LVP line, as indicated by the arrow in Figure 5b.

5 Analysis of Nur and Byerlee experiments

Hereby, VMTPM is applied to the analysis of the kinematics and mechanical state of water saturated sandstone specimens as tested by Nur and Byerlee [21]. Specifically, based on an analysis in EI coordinates of the reported experimental data, the hydro-mechanical conditions effectively applied during experiments are identified. Subsequently, it is shown that EI coordinate analysis also makes possible interpreting and inferring predictions on the nonlinear mechanical response exhibited by this class of poroelastic media.

The tests reported in [21] were carried out by jacketing full water-saturated sandstone specimens of porosity $\phi^{(f)} = 0.06$ in a copper sleeve, and compressing them by a steel plug at controlled flow and pressure. The experimental data set consisted of the confining pressure p^{ext}, the apparent macroscopic volumetric strain of the specimens $\bar{e}^{(s)}$, and the fluid pressure p. Table 1 reports a numerical digitalization of the data reported in Figure 2 of [21]: labels have been added to reference each record of measurements, and the corresponding values of the extrinsic and the intrinsic pressures in EI coordinates have been included operating the coordinates changes $\check{p}^{(s)} = p^{ext} - p$ and $\hat{p}^{(s)} = \phi^{(s)}p$, respectively. The corresponding plot of measured extrinsic strain vs. confining pressure is shown in Figure 6. It can be observed that the experimental points are lined up vertically by groups characterized by the same confining pressure (groups are identified by the same letter).

Stress points in EI pressure coordinates $\check{p}^{(s)}$ and $\hat{p}^{(s)}$ are reported in Figure 7a, and follow a pattern similar to that theoretically deduced in Section 4.5 and reported in Figure 5a. Such

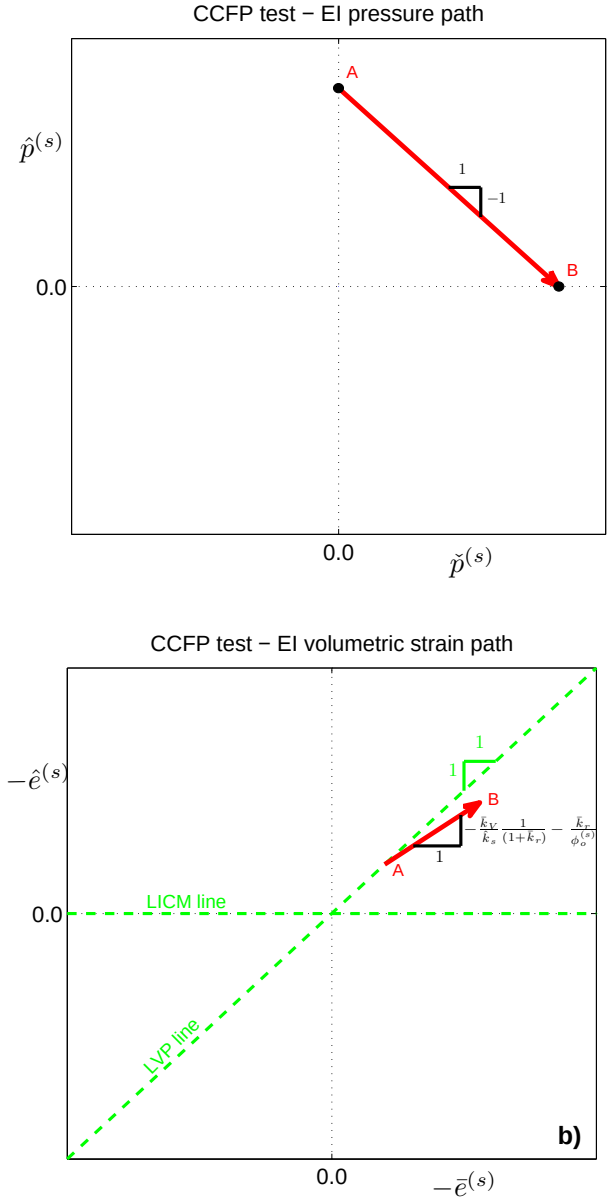

Figure 5: Representation in EI coordinates of the volumetric mechanical response during an ideal creep test with controlled fluid pressure. a) EI pressure path in the $(\hat{p}^{(s)}, \check{p}^{(s)})$ plane; b) EI volumetric strain path in the $(\bar{e}^{(s)}, \hat{e}^{(s)})$ plane. Dotted lines indicate the LVP and LICM limits.

pattern similarity and the constant value of the confining pressure suggest that these experiments are identifiable as CCFP compression tests. The identification of a CCFP test is important since it confirms that the solid stress can be analyzed in terms of simple EI coordinates. Actually, in this test unilateral phenomena have been shown to be not relevant so that deviatoric strains of the solid are easily obtained from their coincidence with the homogeneous deviatoric strain produced in the compressive chamber ($\bar{\boldsymbol{\varepsilon}}^{(s)}_{dev} = \bar{\boldsymbol{\varepsilon}}^{(ext)}_{dev}$), and $\check{\boldsymbol{\sigma}}^{(s)}_{dev} = \boldsymbol{\sigma}^{(ext)}_{dev}$.

	Primary measured quantities			EI pressure coordinates	
label	$\bar{e}^{(s)}$	p^{ext}	p	$\check{p}^{(s)}$	$\hat{p}^{(s)}$
	[-]	[kb]	[kb]	[kb]	[kb]
a1	0.000853	0.26	0.16	0.10	0.15
a2	0.001630	0.26	0.05	0.21	0.05
a3	0.001837	0.26	0.00	0.26	0.00
b1	0.001602	0.51	0.38	0.13	0.36
b2	0.002534	0.52	0.23	0.29	0.22
b3	0.003415	0.51	0.00	0.51	0.00
c1	0.001730	0.62	0.51	0.11	0.48
c2	0.002378	0.62	0.39	0.23	0.37
c3	0.003052	0.62	0.27	0.35	0.25
c4	0.004088	0.63	0.00	0.63	0.00
d1	0.001677	0.84	0.75	0.09	0.70
d2	0.002376	0.83	0.65	0.18	0.61
d3	0.002998	0.83	0.54	0.29	0.51
d4	0.004008	0.84	0.35	0.49	0.33
d5	0.005252	0.84	0.00	0.84	0.00

	Primary measured quantities			EI pressure coordinates	
label	$\bar{e}^{(s)}$	p^{ext}	p	$\check{p}^{(s)}$	$\hat{p}^{(s)}$
	[-]	[kb]	[kb]	[kb]	[kb]
e1	0.002866	1.08	0.86	0.22	0.81
e2	0.003825	1.08	0.69	0.39	0.65
e3	0.004369	1.04	0.52	0.52	0.49
e4	0.005042	1.09	0.41	0.68	0.39
e5	0.006182	1.08	0.00	1.08	0.00
f1	0.004445	1.23	0.81	0.42	0.76
f2	0.005611	1.22	0.47	0.75	0.44
f3	0.006881	1.23	0.00	1.23	0.00
g1	0.005738	1.51	0.85	0.66	0.80
g2	0.006256	1.51	0.65	0.86	0.60
g3	0.007137	1.52	0.32	1.20	0.30
or	0.000000	0.00	0.00	0.00	0.00

Table 1: Confining pressure, p^{ext}, volumetric strain, $\bar{e}^{(s)}$, fluid pressure, p, measured in jacketed compression tests on water saturated Weber sandstone specimens ([21]) and corresponding EI pressure coordinates.

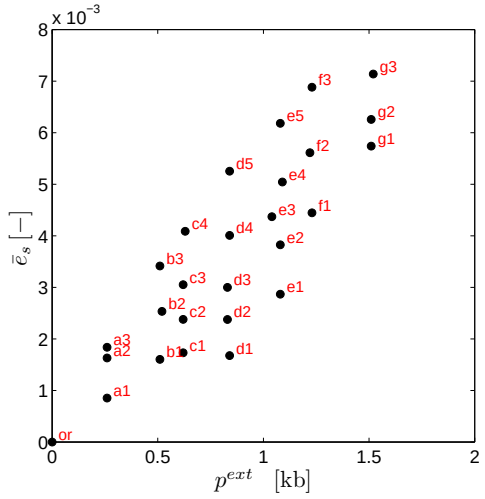

Figure 6: Plot of measured extrinsic strain vs. confining pressure for Weber sandstone specimens (data taken from [21])

In order to represent the corresponding volumetric strain path in EI coordinates, it should be considered that:

- the strain-to-stress response of sandstone exhibits a non negligible nonlinearity. Nur and Byerlee recognized this to be an effect of crack closure, which is a typical feature of compressed sandstones [58]. As originarily observed by the authors, the nonlinearity is specifically pronounced in response to changes of p^{ext} when p is kept fixed, and it is almost absent in response to variations of p alone. Accordingly, this nonlinear response can be described as a secant bulk modulus $\bar{k}_V$ [21], varying as function of the quantity $p^{ext} - p$, viz.: $\bar{k}_V = \bar{k}_V\left(\check{p}^{(s)}\right)$.

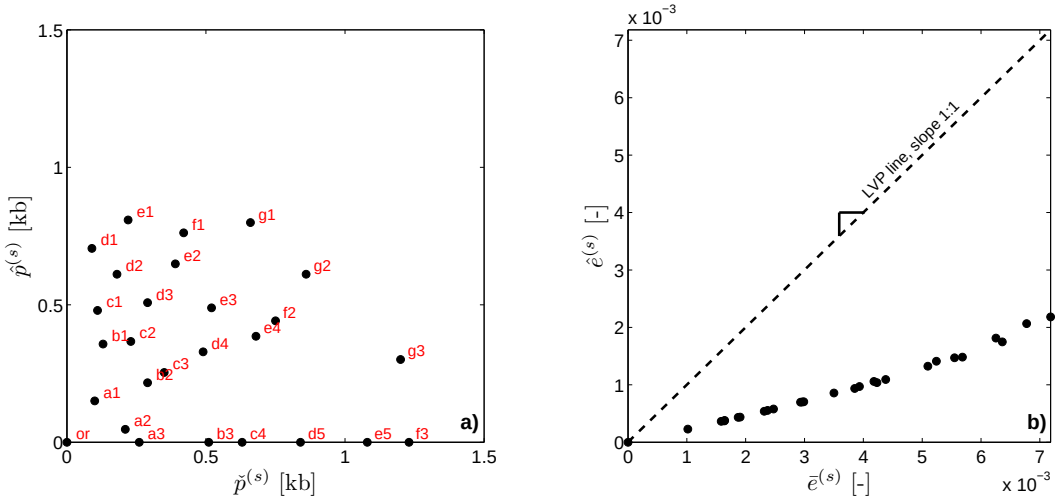

Figure 7: a) Volumetric stress points plotted in the EI pressure coordinate space ($\check{p}^{(s)}$, $\hat{p}^{(s)}$) b) Volumetric strain path in EI coordinates ($\bar{e}^{(s)}$, $\hat{e}^{(s)}$), as estimated by relation (143) from data in [21].

- the intrinsic strain $\hat{e}^{(s)}$ is not among the data reported in [21].

To address such deviations from linearity in EI coordinates, volumetric compliance functions

$$\bar{e}^{(s)} = \bar{e}^{(s)}\left(\check{p}^{(s)}, \hat{p}^{(s)}\right), \qquad \hat{e}^{(s)} = \hat{e}^{(s)}\left(\check{p}^{(s)}, \hat{p}^{(s)}\right) \tag{137}$$

are considered, which generalize to the nonlinear range the linear volumetric compliance relations in EI coordinates represented by equations (40) and (41). The experimental data in Table 1 are used to curve-fit the function $\bar{e}^{(s)} = \bar{e}^{(s)}\left(\check{p}^{(s)}, \hat{p}^{(s)}\right)$ accounting for the above mentioned nonlinear dependence on variable $\check{p}^{(s)}$. Moreover, since no measurement of $\hat{e}^{(s)}$ is reported in [21], its values are extrapolated assuming that the missing information about $\hat{e}^{(s)}$ can be obtained via CSA estimates.

5.1 Determination of $\bar{e}^{(s)}$

An expression of $\bar{e}^{(s)}$ is provided by the first of (41), and reads:

$$\bar{e}^{(s)} = -\frac{1}{\bar{k}_V}\check{p}^{(s)} + \frac{\bar{k}_r}{\phi^{(s)}\bar{k}_V}\hat{p}^{(s)} \tag{138}$$

Aimed at capturing the nonlinear behavior of the rock material with the simplest interpolation, a single quadratic term in the extrinsic pressure is added. Accordingly, the employed interpolating function for $\bar{e}^{(s)}$ reads:

$$-\bar{e}^{(s)} = a_q \left(\check{p}^{(s)}\right)^2 + b_q \check{p}^{(s)} + c_q \hat{p}^{(s)} \tag{139}$$

where a_q, b_q, and c_q are three coefficients. Curve-fitting of the above expression with the experimental data provides:

$$a_q = -0.00188 \text{ [kb}^{-2}\text{]}, \; b_q = 0.00782 \text{ [kb}^{-1}\text{]}, \; c_q = 0.00168 \text{ [kb}^{-1}\text{]}, \tag{140}$$

with a coefficient of determination $R^2 = 0.9979$. The proximity of R to unity indicates the agreement of the experimental data with the proposed model (139), and confirms that $\check{p}^{(s)}$ is the sole stress variable regulating the stiffness changes of the specimens, as originarily observed in [21].

By comparing (138) and (139), the following nonlinear secant expressions for $\bar{k}_V$ and $\bar{k}_r$ are computed:

$$\bar{k}_V = \bar{k}_V \left(\check{p}^{(s)}\right) = \frac{1}{a_q \check{p}^{(s)} + b_q}, \qquad \bar{k}_r = \bar{k}_r \left(\check{p}^{(s)}\right) = -\frac{\phi^{(s)} c_q}{a_q \check{p}^{(s)} + b_q} \tag{141}$$

and, as expected, they turn out to be both nonlinear functions of $\check{p}^{(s)}$ alone, and independent from $\hat{p}^{(s)}$. Within the range of stresses investigated by Nur and Byerlee, $\bar{k}_V$ increases by a ratio of 42 % from 127.9 [kb] to 181.6 [kb], while $\bar{k}_r$ changes from -0.2019 to -0.2867 as $\check{p}^{(s)}$ increases. In particular, it can be observed that (141) yields:

$$\frac{\bar{k}_r}{\phi^{(s)} \bar{k}_V} = -c_q \tag{142}$$

5.2 Estimates of $\hat{e}^{(s)}$

Function $\hat{e}^{(s)} = \hat{e}^{(s)}\left(\check{p}^{(s)}, \hat{p}^{(s)}\right)$ is similarly computed from the second scalar compliance equations provided by (40) and (41). Accordingly, we have:

$$\hat{e}^{(s)} = \frac{\bar{k}_r}{\phi^{(s)} \bar{k}_V} \check{p}^{(s)} - \frac{1}{\phi^{(s)}} \left(\frac{1}{\hat{k}_s} + \frac{\left(\bar{k}_r\right)^2}{\phi^{(s)} \bar{k}_V} \right) \hat{p}^{(s)} \tag{143}$$

where the previously evaluated nonlinear secant interpolations (141) of the experimental data are employed for coefficients $\bar{k}_r$ and $\bar{k}_V$.

Lack of experimental data on $\hat{e}^{(s)}$ for the determination of the remaining macroscopic modulus $\hat{k}_s$ is supplied by a computation via CSA estimates. Accordingly, $\hat{k}_s$ is related to $\bar{k}_r$ and to the microscale shear modulus μ using the estimates in (68):

$$\frac{1}{\hat{k}_s} = -\frac{1-\phi^{(s)}}{\phi^{(s)}} \frac{1}{\frac{4}{3}\mu} \bar{k}_r \qquad \text{(Obtained with CSA)} \tag{144}$$

Regarding the evaluation of μ in (144), it has been reported that the mineralogical components of sandstone (i.e., quartz, calcite and feldspar) are characterized by an almost constant value of the shear modulus [58] for which $\mu = 4.6 \cdot 10^6$ [psi]$= 317.16$ [kb] is taken as an average representative value. Hence, based also on the results of (141) and (140), the magnitude of the term $\frac{1}{\hat{k}_s}$ is estimated to be in the lower range of 10^{-5} [kb^{-1}], making it negligible when compared to the other terms in (143). This is expected since $\hat{k}_s$ diverges in proximity to zero porosity.

The other term $\frac{\bar{k}_r}{\phi^{(s)}\bar{k}_V}$ in (143) has been already computed in (142) to be equal to the constant value $-c_q$, which is independent from $\check{p}^{(s)}$. For this reason its computation does not require subsidiary homogenization estimates. However, it is interesting to observe that its CSA estimate provided by (68) and (69) turns out to be:

$$\frac{\bar{k}_r}{\phi^{(s)}\bar{k}_V} = -\frac{1}{\phi^{(s)}k_s} \qquad \text{(Obtained with CSA)} \tag{145}$$

The above estimate corroborates the property found in (142) that $\frac{\bar{k}_r}{\phi^{(s)}\bar{k}_V}$ is a constant parameter independent of $\check{p}^{(s)}$ and hence unaffected by the nonlinearities of the deformation history during the experiments. Actually, the two terms $\phi^{(s)}$ and k_s are negligibly affected by the nonlinearity of the strain-stress response. In particular, the microscale bulk modulus k_s is a constant microscale parameter which is unaffected by crack closure, a nonlinear phenomenon taking place at a mesoscale level. Also, for the loading conditions applied and the material considered, $\phi^{(s)}$ can be assumed to be constant.

The paths given by (143) are reported in Figure 7 in the volumetric EI coordinates: the experimental data are all aligned along the same curve. This is due to the low porosity of the

sandstone specimens: in the limit of low porosity, the matrix $\left[\bar{C}_{iso}^{(s)}\right]$ in (40) becomes singular at LVP.

The alignment of the data highlights the difficulty in recognizing intrinsic and extrinsic strains to be two *independent* coordinates from the only kinematic point of view in systems having low porosity such as the sandstone specimens. On the other hand, the necessity of addressing the description of sandstone specimens in terms of two independent volumetric stress and strain coordinates is undeniably recognized. Actually, the examined experimental data have shown that, in these poroelastic systems, strain and stiffness depend on both $\check{p}^{(s)}$ and $\hat{p}^{(s)}$ (see (138), and (141)). Such dependency cannot be lumped into one single stress variable governing both strain and stiffness. Moreover, the convenience of analyzing the strain response in terms of two strain variables ($\bar{e}^{(s)}$, $\hat{e}^{(s)}$) can be appreciated in Figure 7b: as the deformation increases, the trend of the strain path is to incline towards the direction of the LVP line, which represents an insuperable upper bound for the inclination of the curves in the space ($\bar{e}^{(s)}$, $\hat{e}^{(s)}$) as discussed in Section 4. Such tendency of the EI volumetric strain path to increase its slope towards the direction of the LVP line can be interpreted as the effect of crack closures and, more generally, as a characteristic nonlinear behavior of compacting materials.

6 Domain of validity of Terzaghi's principle according to VMTPM

In the light of the results presented in Sections 4 and 5, it is possible to conduct an analysis in EI coordinates on the range of validity of Terzaghi's effective stress principle as a trustworthy stress partitioning law generally applicable to fluid saturated porous media. The notion of *single* effective stress is of great historical importance in application of porous media theories to geomechanics [59–61]. Besides, it is also of substantial practical engineering convenience for general constitutive modelling purposes since, when applicable, it allows to connect back the behavior of a porous medium in a multiphase environment to the response of the solid phase alone, treated as a single-phase continuum.

With specific reference to soils, Terzaghi refers to the effective stress as: "*All the measurable effects of a change of stress, such as compression, distortion and a change in the shearing resistance are exclusively due to changes in effective stresses*" [62]. Later on, the concept of effective stress has been extended and examined in relation to specific observable effects such

as strain [11–13] and strength [9, 14, 15] properties; also, it has been used for describing the behavior of rocks and partially saturated soils [4, 21, 63], as well as bone [16] and cartilage [18] tissues. In the following, it is shown how Terzaghi's statement can be actually inferred as a prediction of VMTPM for cohesionless frictional granular materials such as soils. Subsequently, the implications of the recovery of the Terzaghi's principle in relation to the mechanical response observed in media different from soils (e.g., rocks) is discussed.

6.1 Recovery of Terzaghi's law for cohesionless frictional granular materials

In granular materials, compressing deformation typically occurs at the expense of intergranular pore space [61]. This implies that the extrinsic strain is much larger than the intrinsic one (i.e., $\bar{e}^{(s)} >> \hat{e}^{(s)}$). Hence, evaluation of $\bar{k}_r$ by a JD test yields $\bar{k}_r = -\phi^{(s)}\frac{\hat{e}^{(s)}}{\bar{e}^{(s)}} \simeq 0$, see (92). In the condition of a vanishing $\bar{k}_r$, the extrinsic and intrinsic strains become decoupled. This is inferred from (43) for $\bar{e}^{(s)}$, and from (40) and (41) for $\hat{e}^{(s)}$ (see also (143)). So we have:

$$\bar{k}_r = 0, \qquad \bar{\boldsymbol{\varepsilon}}^{(s)} = \frac{1+\bar{\nu}}{\bar{E}}\check{\boldsymbol{\sigma}}^{(s)} - \frac{\bar{\nu}}{\bar{E}}\mathrm{tr}\check{\boldsymbol{\sigma}}^{(s)}\,\boldsymbol{I}, \qquad \hat{e}^{(s)} = -\frac{1}{\phi^{(s)}\hat{k}_s}\hat{p}^{(s)} \tag{146}$$

Most importantly, the extrinsic strain, which is normally the primary strain object of measure, becomes dependent exclusively on the extrinsic stress tensor $\check{\boldsymbol{\sigma}}^{(s)}$.

Furthermore, the results shown in this study indicate that, for those materials such as cohesionless granular materials whose strength and/or stiffness properties are determined by contact over interior surfaces, strain ($\bar{\boldsymbol{\varepsilon}}^{(s)}$), strenght and stiffness are solely governed by the stress variable $\check{\boldsymbol{\sigma}}^{(s)}$, with $\hat{p}^{(s)}$ having a negligible effect.

An experimental evidence of the insensitiveness of interior contacting interfaces to changes of $\hat{p}^{(s)}$ can be deduced from the stiffening in sandstone specimens. As shown in Section 5.2, $\hat{p}^{(s)}$ has no effect on stiffness. Accordingly, since stiffening in sandstones is known to be an effect of crack closure [58], it is deduced that $\check{p}^{(s)}$ is the only stress variable responsible for increase or decrease of contact across interior surfaces. This property finds also a rational justification in light of the results of Section 4.3 concerning the response to an unjacketed test, where it is deduced that an increment in the intrinsic stress alone induces a homothetic strain response ($\bar{e}^{(s)} = \hat{e}^{(s)}$) in a two-phase medium. Since the homothety preserves a similitude between the shapes of the solid domain before and after deformation takes place, it does not alter the quota

of interior surfaces in open-contact or closed-contact conditions.

Hence, for cohesionless frictional granular materials for which both condition (146) and insensitivity to $\hat{p}^{(s)}$ apply (e.g., soils), the observed effects comply with Terzaghi's statement if $\hat{e}^{(s)}$ is excluded from the measured effects of stress changes. The corresponding relations recovered by VMTPM between primary observed volumetric quantities and external spherical loadings p^{ext} and p are collected from the previous sections (see (11), (32), (80), $(141)_1$ and the trace of (146)) in synoptic form:

$$\check{p}^{(s)} = p^{ext} - p, \qquad \check{p}^{(s)} = -\frac{1}{3}\mathrm{tr}\check{\boldsymbol{\sigma}}^{(s)} \tag{147}$$

$$\bar{e}^{(s)} = -\frac{1}{\bar{k}_V}\check{p}^{(s)}, \qquad \bar{k}_V = \bar{k}_V\left(\check{p}^{(s)}\right) \tag{148}$$

$$\frac{\partial \check{\sigma}_{ij}^{(s)}}{\partial x_j} - \phi^{(s)}\frac{\partial p}{\partial x_i} + \bar{b}_i^{(sf)} + \bar{b}_i^{(s,ext)} = 0 \tag{149}$$

To point out the significance of relations (147)-(149) within VMTPM, three important properties must be remarked:

- The extrinsic stress tensor $\check{\boldsymbol{\sigma}}^{(s)}$ in equation (147) is not just a stress variable introduced for constitutive purposes, but it is actually the *same* stress quantity entering the linear momentum balance of the solid phase (see equation (11)), recalled by the second equation in (149) for statics.

- Relations (147)-(149) hold for media with finite volumetric compressibility of the solid and fluid constituent materials. In this respect, it is important to recall that, as classically demonstrated (see for instance [11–13]), recovery of compliance with Terzaghi's statement can be also put in connection with the stronger hypothesis that the constituent solid material is volumetrically incompressible. In such a limit of volumetrically incompressible constituent solid material (LICM) (corresponding to $\dfrac{\mu}{k_s} \to 0$, or equivalenty to $\nu \to 0.5$, it can be inferred from estimates (68)-(70) that $\frac{1}{\bar{k}_s} \to 0$ and $\bar{k}_r \to 0$, while $\bar{k}_V$ retains a finite value. Under this hypothesis, a specialization even stronger than (146) is obtained, which yields $\hat{e}^{(s)} = 0$. Accordingly, for frictional granular materials, when an *ad-hoc* LICM hypothesis is added, all macroscopically observable effects become truly dependent only on $\check{p}^{(s)}$, since $\hat{e}^{(s)}$ is strictly zero and $\hat{p}^{(s)}$ has a negligible effect on shear

strength and stiffness. In contrast, within VMTPM, the property of low $\bar{k}_r$ is completely independent from the microscale stiffness parameters μ and k_s, which can retain finite values even when $\bar{k}_r = 0$. This makes possible an ordinary employment of VMTPM for wave propagation analysis also in cohesionless granular materials, since singularities in the wave speed are avoided.

- From a formal point of view, relation (147) exactly matches with Terzaghi's stress partitioning law. Nevertheless, while this formula was originarily introduced by Terzaghi with the purpose of condensing all observed experimental mechanical effects over soils, the significance of (147) in VMTPM is much more general and *not* confined to soils alone. Actually, in VMTPM, equation (147) stems directly from (20), which is obtained based on a derivation which is variationally consistent and *medium-independent* (i.e., in absence of any hypothesis on the microstructure or of constitutive type) [37]. As such, relation (147) is also independent from the microstructural realizaton of a given medium, and from any constitutive hypothesis such as intrinsic volumetric incompressibility. Hence, as observed in [10], compliance with (147) reflects a fundamental medium-independent equilibrium property rooted in the least Action principle, and thus holding regardless of the microstructure. In this respect, a parallel can be drawn with the property of symmetry of the stress tensor, which similarly reflects the fundamental rotational equilibrium and also holds irrespective of the microstructure.

6.2 Extensibility of Terzaghi's effective stress and Terzaghi's principle beyond cohesionless granular materials

For classes of media other than cohesionless granular materials, the veracity of Terzaghi's principle, as expressed by (148)-(149), has to be assessed case by case. Similarly, the extensibility of Terzaghi's principle (i.e. the possibility of condensing the dependence of all observed effects upon a single stress variable) has to be assessed considering the specific nature of the mechanical response of the class of media examined.

For saturated sandstone rocks, as observed in Section 5.2, a significant deviation from (148) is found. This is because the strain-confinement pressure-fluid pressure relation measured in [21] results into the law $p^{ext} = -\bar{k}_V \bar{e}_b^{(s)} + \alpha p_b$ with α far from a unit value. Such a deviation is

theoretically confirmed as an ordinary prediction of VMTPM, see relation (85) when $\bar{k}_r$ is not zero. Furthermore, this study reveals an even stronger agreement with the estimate obtained by Nur and Byerlee for α, which they found to be experimentally well fitted by $\alpha = 1 - \bar{k}_V/k_s$. Actually, as shown in Section 4, the combination of these last two relations can be also theoretically inferred from (85) when CSA estimates are employed to relate microscale and macroscopic stiffness moduli (see Eqs.(85) and (88)).

Turning to the search for a single effective stress regulating all observable effects in water saturated sandstones, it can be recognized that a single volumetric stress coordinate regulating both strain and stiffness in these media cannot be found. The choice most frequently encountered in the literature (and also adopted in [21]) for generalizing the notion of effective stress in order to accomodate the deviation from Terzaghi's law is to replace it with the isostrain stress $p^{\bar{e}^{(s)}}$. This last stress quantity is defined as the confining stress that should be externally applied to the same specimen, upon drying it, to induce the same macroscopic strain produced by the concomitant action of p and $\check{p}^{(s)}$, viz:

$$p^{\bar{e}^{(s)}}: \qquad \bar{e}^{(s)} = -\frac{1}{\bar{k}_V} p^{\bar{e}^{(s)}} \tag{150}$$

This definition yields, on account of (10) and (138), the following expression for $p^{\bar{e}^{(s)}}$:

$$p^{\bar{e}^{(s)}} = \check{p}^{(s)} - \bar{k}_r p = p^{ext} - \left(1 + \bar{k}_r\right) p \tag{151}$$

which, as opposite to $(147)_1$, is manifestly driven by the microstructure, since it contains $\bar{k}_r$.

While this modification of effective stress into $p^{\bar{e}^{(s)}}$ is capable of restoring the dependency of volumetric strain upon a single stress variable, as already pointed out by Nur and Byerlee and confirmed by the analysis carried out in Section 5.2 (see equation (141)), the stiffness of the saturated speciments does not depend on $p^{\bar{e}^{(s)}}$ alone. In fact, it is solely regulated by the other volumetric stress coordinate $\check{p}^{(s)}$, being insensitive to $\hat{p}^{(s)}$. It is thus concluded that all the macroscopically observable mechanical effects in sandstone cannot be regulated by $p^{\bar{e}^{(s)}}$ alone. In this respect, the inadequacy of the isostrain stress for assessing the strength of several classes of saturated porous materials has been previously observed, and it has been specifically

discussed (see for instance [9]).

In conclusion, for rock materials and other classes of biphasic porous media which do not belong to the family of cohesionless granular materials, neither the extrinsic stress $\check{p}^{(s)}$ nor the isostrain stress $p^{\bar{e}^{(s)}}$ can adequately be employed to lump the dependence of all mechanically significant observable effects into a single effective stress variable.

A generalization of Terzaghi's principle urges a dependency upon two volumetric stress coordinates at least. Within the framework of VMTPM, the natural two-coordinate extension of the classical statement of Terzaghi's principle, encompassing all theoretical and experimental results herein discussed, is represented by an extension of the dependency of all observable mechanical effects upon all DEI stress coordinates $\check{\boldsymbol{\sigma}}^{(s)}_{dev}$, $\hat{p}^{(s)}$ and $\check{p}^{(s)}$. Actually, these coordinates represent the privileged choice for defining a volumetric stress state in VMTPM, being $\hat{p}^{(s)}$ and $\check{p}^{(s)}$ the stresses work-associated with primary volumetric strain variables of the solid phase ($\bar{e}^{(s)}$ and $\hat{e}^{(s)}$). Accordingly, the following generalized statement is proposed:

Generalized Terzaghi's principle:

"*All the measurable mechanical effects over the solid porous phase produced by a change of stresses in a multi-phase porous medium are exclusively due to changes in DEI coordinates, i.e., in the deviatoric stress tensor and in the extrinsic and intrinsic pressures.*"

The classical statement for soils, represented by (147)-(149), is only recovered as a specialization of the above statement for the subclass of cohesionless granular materials. In this case the insensitivity to the intrinsic pressure makes the observable effects solely driven by the extrinsic stress tensor.

7 Discussions and Conclusions

Stress partitioning between solid and fluid phases in fluid saturated porous media is complex and yet not completely understood. In this study, the variational continuum poroelastic framework VMTPM was adopted to derive general procedures and operative formulas for the analysis of stress partitioning in biphasic systems subjected to compression in both drained and undrained conditions. VMTPM provides a suitable ground for stress partitioning analysis since it only employs stress variables which are ordinarily defined in terms of explicit work-association with primary strain variables, with no use of Lagrange multipliers.

In Part I [37], local strong form of boundary conditions and conditions holding at solid-fluid interfaces were derived based on a variational analysis. These conditions have been combined in Section 2 to address unilateral contact over a binary solid-fluid mixture (by Equations (18)) via a simple extension of the use of a set-valued law and a gap function ordinarily employed in single-phase contact theories. Such boundary conditions allow addressing, in a variationally-consistent and medium-independent macroscopic continuum treatment, a large class of boundary value poroelastic problems without invoking further mechanical arguments.

In Section 3.2 it is shown that, under hypotheses of isotropy, VMTPM momentum balance equations recover the structure of Biot's equations. Such a recovery is notable since VMTPM proceeds from a purely variational statement of the poroelastic two-phase problem while previous works, see, e.g., [64], have argued the difficulty of obtaining Biot's equations proceeding from a variational principle, motivated by the presence of a nonequilibrium variable, the increment of fluid content, in Biot's derivation of governing equations. The variational statement of the problem considered in VMTPM does not contain, however, nonequilibrium variables in the kinematic description. Explicit expressions for the elastic coefficient entering these Biot-like equations, as function of the elastic moduli of individual phases, are also obtained in Section 3.2. However, an important difference with Biot's framework is the retrieval of a positive increment of a stiffness coefficient entering the solid linear momentum balance with respect to the corresponding term of Biot's theory (*added stiffness*). The magnitude of this coefficient which seems to have been overlooked in Biot's theory, appears to be non-negligible in most applications. In contrast, in the medium-independent equations herein considered, no *added mass* coefficients appear. A further element of reciprocal corroboration between VMTPM and Biot's theory is the identification of the relationship $\bar{k}_r = \alpha - 1$ between the constitutive dimensionless ratio $\bar{k}_r$ of VMTPM and Biot's coefficient α.

The capability of VMTPM of addressing a comprehensive variety of boundary and surface conditions was exploited to perform a comprehensive analysis of the mechanical responses of biphasic specimens during JD, U, JU and CCFP static compression tests, see Section 4. This was carried out with no limitation on porosity and/or other material properties (e.g. compressibility, permeability, etc.). The four examined testing conditions offered a broad scope of compression histories, which can be used for the mechanical identification of a wide range of experimental

conditions. Hence, the deriving results can be deployed for investigating various porous media applications.

These elemental responses were subsequently employed in Section 5 for identifying the hydro-mechanical conditions determined by the experimental set-up of Nur and Byerlee during their compression tests on Weber sandstone specimens [21], which is generally regarded as a proof of deviation from Terzaghi's effective stress principle. It was shown that the experimental conditions in which the specimen were tested corresponded to those of a CCFP compression test, and that the peculiar behavior of this soil can be actually predicted by VMTPM. In particular, the Weber sandstone response to CCFP compression was analyzed in terms of primary observed quantities (p^{ext}, p, and $\bar{e}^{(s)}$) via relations (85)-(88), and also accounting for the nonlinear response of volumetric stress and strain paths, see Figures 7.

An appropriate selection of independent primary stress variables or single effective stress is of special relevance for constitutive modeling of unsaturated soils [4, 63]. Within VMTPM, privileged stress coordinates are naturally identified in DEI coordinates. Specifically, DEI strain coordinates consist of the deviatoric strain $\bar{\boldsymbol{\varepsilon}}^{(s)}_{dev}$ plus the volumetric extrinsic and intrinsic strains ($\bar{e}^{(s)}$), ($\hat{e}^{(s)}$), while DEI stress coordinates consist of the corresponding work-associated variables $\check{\boldsymbol{\sigma}}^{(s)}_{dev}$, $\check{p}^{(s)}$ and $\hat{p}^{(s)}$.

DEI coordinates were used to track the poroelastic response to ideal JD, U, JU, CCFP compression tests, and for predicting and interpreting the experimental data reported in [21], see Section 5.2. In particular, when DEI coordinates were adopted to analyze the JU test, it was shown how the phenomenon of compression-induced liquefaction, experimentally observed in sands [56] and deemed responsible for blast-induced liquefaction, results to be a natural theoretical prediction of VMTPM for cohesionless materials. Such prediction emerges naturally (i.e., without adding ad-hoc constitutive features to describe compression-induced liquefaction) when the unilateral character of cohesionless materials is taken into account, see Section 4.4. Actually, discriminated by the specific values of stiffness moduli of the solid phase and of the interstitial fluid in a given cohesionless mixture, three distinct behaviors were identified and classified into *nonliquefying*, *partially liquefying* and *full liquefying* cohesionless mixtures. In this respect, it is important to remark that, although liquefaction is mostly known to be associated with laboratory and in situ conditions, as an effect essentially induced by deviatoric undrained loading

and excitations, there exist experimental evidences indicating that sands can be also liquefied by isotropic compressive stress applied under quasistatic drained conditions. Moreover, DEI coordinates were also deployed to predict the effective stress law experimentally determined in [21], and when interpreting the nonlinear features of the experimental data set reported therein, see Section 5.2. Specifically, the stiffening in sandstone specimen due to crack closure was recognized to be reflected by a reorientation of the strain curve in EI coordinates, which tends to align along the LVP line.

Finally, In Section 6, on the basis of the results of Sections 4 and 5, it was shown that:

- when VMTPM is specialized to describe media with granular microstructure and cohesionless behavior of the solid phase, the resulting poroelastic theory is characterized by full compliance with Terzaghi's stress partitioning law: this theory actually predicts that both macroscopic strain and stiffness are solely dependent on $\check{p}^{(s)}$, and insensitive to $\hat{p}^{(s)}$, so that $\check{\boldsymbol{\sigma}}^{(s)}$ assumes the role of the *effective stress* (i.e., a stress quantity regulating all macroscopically observable effects on the solid phase);

- such specialized poroelastic theory (i.e., under the hypotheses of granular microstructure and cohesionless behavior) entails no incompressibility constraint; therefore, it can be applied to wave propagation analysis in saturated granular solids, such as soils;

- when the hypotheses of granular microstructure and cohesionless behavior are removed, as in the case of sandstone rocks, VMTPM predicts that a generalization of Terzaghi's principle, with a single stress coordinates regulating all observable effects, is not feasible; consequently, a generalization of dependence upon more than one stress coordinate becomes mandatory;

- a generalized statement of Terzaghi's principle was proposed for multiphase problems, postulating that changes of DEI coordinates are responsible for all macroscopically measurable mechanical effects on the solid phase produced by loading.

Altogether the applications shown in this contribution have exemplified the capability of VTMPM to describe and predict a large class of linear and nonlinear mechanical behaviors observed in two-phase saturated materials. Future applications of VMTPM will be directed towards the assessment of its capability to describe, upon introducing suitable constitutive hypotheses,

responses stemming from volumetric-deviatoric coupling such as dilatancy in geomaterials, as well its predictive features in combination with elastoplastic constitutive laws.

References

[1] P. Fillunger, Versuche über die zugfestigkeit bei allseitigem wasserdruck, Osterr. Wochenschr. Offentl. Baudienst 29 (1915) 443–448.

[2] K. Terzaghi, The shearing resistance of saturated soils and the angle between the planes of shear, International Conference on Soil Mechanics and Foundation Engineering, Cambridge (MA), USA.

[3] A. Skempton, Terzaghi's discovery of effective stress, From Theory to Practice in Soil Mechanics: Selections from the Writings of Karl Terzaghi (1960) 42–53.

[4] M. Nuth, L. Laloui, Effective stress concept in unsaturated soils: clarification and validation of a unified framework, International Journal for Numerical and Analytical Methods in Geomechanics 32 (7) (2008) 771–801.

[5] R. Jardine, A. Gens, D. Hight, M. Coop, Developments in understanding soil behaviour, in: Advances in geotechnical engineering: The Skempton conference, Thomas Telford, 2004, p. 103.

[6] R. M. Bowen, Compressible porous media models by use of the theory of mixtures, International Journal of Engineering Science 20 (6) (1982) 697–735.

[7] O. Coussy, L. Dormieux, E. Detournay, From mixture theory to Biot's approach for porous media, International Journal of Solids and Structures 35 (34) (1998) 4619–4635.

[8] R. de Boer, W. Ehlers, The development of the concept of effective stresses, Acta Mechanica 83 (1-2) (1990) 77–92.

[9] P. De Buhan, L. Dormieux, On the validity of the effective stress concept for assessing the strength of saturated porous materials: a homogenization approach, Journal of the Mechanics and Physics of Solids 44 (10) (1996) 1649–1667.

[10] R. Serpieri, F. Travascio, S. Asfour, L. Rosati, Variationally consistent derivation of the stress partitioning law in saturated porous media, International Journal of Solids and Structures 56-57 (2015) 235–247.

[11] M. A. Biot, Theory of elasticity and consolidation for a porous anisotropic solid, Journal of Applied Physics 26 (2) (1955) 182–185.

[12] O. Coussy, Mechanics of porous continua, Wiley, 1995.

[13] J. R. Rice, M. P. Cleary, Some basic stress diffusion solutions for fluid-saturated elastic porous media with compressible constituents, Reviews of Geophysics and Space Physics 14 (2) (1976) 227–241.

[14] S. Pietruszczak, G. Pande, On the mechanical response of saturated cemented materials - part i: theoretical considerations, International Journal for Numerical and Analytical Methods in Geomechanics 19 (8) (1995) 555–562.

[15] S. Pietruszczak, G. Turu, G. Pande, On the mechanical response of saturated cemented materials - part ii: experimental investigation and numerical simulations, International Journal for Numerical and Analytical Methods in Geomechanics 19 (8) (1995) 563–571.

[16] C. Hellmich, F.-J. Ulm, Drained and undrained poroelastic properties of healthy and pathological bone: a poro-micromechanical investigation, Transport in Porous Media 58 (3) (2005) 243–268.

[17] V. Mow, S. Kuei, W. Lai, C. Armstrong, Biphasic creep and stress relaxation of articular cartilage in compression: theory and experiments, Journal of Biomechanical Engineering 102 (1) (1980) 73–84.

[18] A. Oloyede, N. Broom, Complex nature of stress inside loaded articular cartilage, Clinical Biomechanics 9 (3) (1994) 149–156.

[19] V. C. Mow, R. Huiskes, Basic orthopaedic biomechanics & mechano-biology, Lippincott Williams & Wilkins, 2005.

[20] M. Biot, D. Willis, The elastic coefficients of the theory of consolidation, Journal of Applied Mechanics 24 (1957) 594–601.

[21] A. Nur, J. Byerlee, An exact effective stress law for elastic deformation of rock with fluids, Journal of Geophysical Research 76 (26) (1971) 6414–6419.

[22] A. Bishop, The influence of an undrained change in stress on the pore pressure in porous media of low compressibility, Geotechnique 23 (3).

[23] W. G Gray, B. A Schrefler, Analysis of the solid phase stress tensor in multiphase porous media, International Journal for Numerical and Analytical Methods in Geomechanics 31 (4) (2007) 541–581.

[24] P. Lade, R. De Boer, The concept of effective stress for soil, concrete and rock, Geotechnique 47 (1) (1997) 61–78.

[25] A. Bedford, D. Drumheller, A variational theory of porous media, International Journal of Solids and Structures 15 (12) (1979) 967–980.

[26] A. Bishop, The effective stress principle, Teknisk Ukeblad 39 (1959) 859–863.

[27] R. de Boer, Theoretical poroelasticity – a new approach, Chaos, Solitons & Fractals 25 (4) (2005) 861–878.

[28] W. G. Gray, S. M. Hassanizadeh, Unsaturated flow theory including interfacial phenomena, Water Resources Research 27 (8) (1991) 1855–1863.

[29] W. G. Gray, B. A. Schrefler, F. Pesavento, The solid phase stress tensor in porous media mechanics and the hill–mandel condition, Journal of the Mechanics and Physics of Solids 57 (3) (2009) 539–554.

[30] R. Lancellotta, Coupling between the evolution of a deformable porous medium and the motion of fluids in the connected porosity, in: Porous Media, Springer, 2002, pp. 199–225.

[31] B. Schrefler, Mechanics and thermodynamics of saturated/unsaturated porous materials and quantitative solutions, Applied Mechanics Reviews 55 (4) (2002) 351–388.

[32] K. Wilmanski, On microstructural tests for poroelastic materials and corresponding Gassmann-type relations, Geotechnique 54 (9) (2004) 593–603.

[33] B. Albers, K. Wilmański, Influence of coupling through porosity changes on the propagation of acoustic waves in linear poroelastic materials, Archives of Mechanics 58 (4-5) (2006) 313–325.

[34] M. Goodman, S. Cowin, A continuum theory for granular materials, Archive for Rational Mechanics and Analysis 44 (4) (1972) 249–266.

[35] M. Hassanizadeh, W. G. Gray, General conservation equations for multi-phase systems: 1. averaging procedure, Advances in Water Resources 2 (1979) 131–144.

[36] K. Wilmanski, A thermodynamic model of compressible porous materials with the balance equation of porosity, Transport in Porous Media 32 (1) (1998) 21–47.

[37] R. Serpieri, F. Travascio, A purely-variational purely-macroscopic theory of two-phase porous media – part i: Derivation of medium-independent governing equations and stress partitioning laws, Submitted.

[38] R. Serpieri, L. Rosati, Formulation of a finite deformation model for the dynamic response of open cell biphasic media, Journal of the Mechanics and Physics of Solids 59 (4) (2011) 841–862.

[39] R. Serpieri, A rational procedure for the experimental evaluation of the elastic coefficients in a linearized formulation of biphasic media with compressible constituents, Transport in Porous Media 90 (2) (2011) 479–508.

[40] R. Serpieri, F. Travascio, General quantitative analysis of stress partitioning and boundary conditions in undrained biphasic porous media via a purely macroscopic and purely variational approach, Continuum Mechanics and Thermodynamics 28 (1-2) (2016) 235–261.

[41] F. Travascio, S. Asfour, R. Serpieri, L. Rosati, Analysis of the consolidation problem of compressible porous media by a macroscopic variational continuum approach, Mathematics and Mechanics of Solids (2015) DOI: 1081286515616049.

[42] R. Serpieri, F. Travascio, S. Asfour, Fundamental solutions for a coupled formulation of porous biphasic media with compressible solid and fluid phases, in: Computational Methods for Coupled Problems in Science and Engineering V –A Conference Celebrating the 60th Birthday of Eugenio Onate, COUPLED PROBLEMS, 2013, pp. 1142–1153.

[43] F. Travascio, R. Serpieri, S. Asfour, Articular cartilage biomechanics modeled via an intrinsically compressible biphasic model: Implications and deviations from an incompressible biphasic approach, in: ASME 2013 Summer Bioengineering Conference, American Society of Mechanical Engineers, 2013, pp. V01BT55A004–V01BT55A004.

[44] ASTM standard d 2435-96. standard test method for one-dimensional consolidation properties of soils. Annual book of ASTM standards 04.08.

[45] C. Armstrong, W. Lai, V. Mow, An analysis of the unconfined compression of articular cartilage, Journal of Biomechanical Engineering 106 (2) (1984) 165–173.

[46] P. Wriggers, T. A. Laursen, Computational contact mechanics, Vol. 30167, Springer, 2006.

[47] C. Studer, Numerics of unilateral contacts and friction: modeling and numerical time integration in non-smooth dynamics, Vol. 47, Springer Science & Business Media, 2009.

[48] Z. Hashin, The elastic moduli of heterogeneous materials, Journal of Applied Mechanics 29 (1) (1962) 143–150.

[49] Z. Hashin, Analysis of composite materials – a survey, Journal of Applied Mechanics 50 (3) (1983) 481–505.

[50] M. A. Biot, Theory of propagation of elastic waves in a fluid-saturated porous solid. I. Low-frequency range, The Journal of the Acoustical Society of America 28 (2) (1956) 168–178.

[51] B. Markert, A constitutive approach to 3-d nonlinear fluid flow through finite deformable porous continua, Transport in Porous Media 70 (3) (2007) 427–450.

[52] K. Lee, R. Westmann, Elastic properties of hollow-sphere-reinforced composites, Journal of Composite Materials 4 (2) (1970) 242–252.

[53] M. A. Biot, General theory of three-dimensional consolidation, Journal of Applied Physics 12 (2) (1941) 155–164.

[54] S. L. Kramer, H. B. Seed, Initiation of soil liquefaction under static loading conditions, Journal of Geotechnical Engineering 114 (4) (1988) 412–430.

[55] T. Youd, I. Idriss, R. D. Andrus, I. Arango, G. Castro, J. T. Christian, R. Dobry, W. L. Finn, L. F. Harder Jr, M. E. Hynes, et al., Liquefaction resistance of soils: summary report from the 1996 NCEER and 1998 NCEER/NSF workshops on evaluation of liquefaction resistance of soils, Journal of geotechnical and geoenvironmental engineering.

[56] R. J. Fragaszy, M. E. Voss, Undrained compression behavior of sand, Journal of Geotechnical Engineering 112 (3) (1986) 334–347.

[57] A. Skempton, The pore-pressure coefficients a and b, Geotechnique 4 (4) (1954) 143–147.

[58] R. W. Zimmerman, Compressibility of sandstones, Elsevier, 1990.

[59] K. v. Terzaghi, Die berechnung der durchlassigkeitsziffer des tones aus dem verlauf der hydrodynamischen spannungserscheinungen, Sitzungsberichte der Akademie der Wissenschaften in Wien, Mathematisch-Naturwissenschaftliche Klasse, Abteilung IIa 132 (1923) 125–138.

[60] A. Skempton, Effective stress in soils, concrete and rocks, Selected papers on soil mechanics 1032 (1984) 4–16.

[61] R. Lancellotta, Geotechnical engineering, CRC Press, 2008.

[62] K. v. Terzaghi, The shearing resistance of saturated soils and the angle between the planes of shear, in: Proceedings of the 1st international conference on soil mechanics and foundation engineering, Vol. 1, Harvard University Press Cambridge, MA, 1936, pp. 54–56.

[63] D. G. Fredlund, N. R. Morgenstern, Stress state variables for unsaturated soils, Journal of Geotechnical and Geoenvironmental Engineering 103 (ASCE 12919).

[64] K. Wilmanski, A few remarks on Biot's model and linear acoustics of poroelastic saturated materials, Soil Dynamics and Earthquake Engineering 26 (6) (2006) 509–536.

8 List of Symbols

Vector and tensor quantities are notated in bold. Null vector quantities and null tensor quantities are indicated by $\mathbf{o}$ and $\mathbf{O}$, respectively. Gibbs nabla vector ∇ is used, when necessary, for implicit shorthand representation of differential operations. For all microscale quantities, of kinematic, stress and stiffness type, no accent is used. In general, an overbar is used to denote macroscopic kinematic quantities, except for kinematic quantities of *intrinsic* type which are denoted by a hat accent. Macroscopic stress quantities are all notated with accents different from the overbar, with the only exceptions of macroscopic Cauchy stresses and of the fluid pressure which have no accent. Intrinsic macroscopic stresses are denoted by a hat accent while extrinsic macroscopic stresses are denoted by a check accent (a reversed hat). In general, subscripts indicate the Cartesian indexes of scalar components. The phase to which a given quantity belongs is denoted by bracketed superscripts s or f, if not otherwise stated. Specific items used in the paper are listed in the following tables.

Symbol	Description
$\Omega^{(M)}$	macroscopic domain of the mixture
$\Omega^{(s)}$	macroscopic subset domain of the mixture with nonvanishing solid phase
$\Omega^{(f)}$	macroscopic subset domain of the mixture entirely occupied by the fluid
$\mathcal{S}^{(sf)}$	free solid-fluid macroscopic interface in the current configuration
$\mathbf{X}$	generic point of the macroscopic reference domain of the mixture
$\mathbf{x}$	generic point of the macroscopic current domain of the mixture
$\bar{\boldsymbol{\chi}}^{(s)}$	macroscopic placement vector of the solid phase
$\bar{\boldsymbol{\chi}}^{(f)}$	macroscopic placement vector of the fluid phase
$\Phi_0^{(s)}$	reference solid volume fraction
$\Phi_0^{(f)}$	reference fluid volume fraction
$\phi^{(s)}$	current solid volume fraction
$\phi^{(f)}$	current fluid volume fraction
$\hat{J}^{(s)}$	finite macroscopic intrinsic volumetric strain of the solid phase
$\bar{J}^{(s)}$	finite macroscopic extrinsic volumetric strain of the solid phase
$J^{(f)}$	finite microscale volumetric strain of the fluid phase
$\hat{\rho}_0^{(s)}$	macroscopic true density of the solid phase in the reference configuration
$\hat{\rho}^{(s)}$	macroscopic true density of the solid phase in the current configuration
$\bar{\rho}^{(s)}$	apparent solid density
$\bar{\rho}^{(f)}$	apparent fluid density

Table 2: List of symbols

Symbol	Description
$\bar{\mathbf{u}}^{(s)}$	infinitesimal macroscopic displacement vector of the solid phase
$\bar{\mathbf{u}}^{(f)}$	infinitesimal macroscopic displacement vector of the fluid phase
$\hat{e}^{(s)}$	infinitesimal macroscopic intrinsic volumetric strain of the solid phase
$\hat{e}^{(f)}$	infinitesimal macroscopic intrinsic volumetric strain of the fluid phase
$\bar{e}^{(s)}$	infinitesimal macroscopic extrinsic volumetric strain of the solid phase
$\bar{e}^{(f)}$	infinitesimal macroscopic extrinsic volumetric strain of the fluid phase
$\bar{\boldsymbol{\varepsilon}}^{(s)}$	infinitesimal extrinsic strain tensor
$\bar{\psi}^{(s)}$	apparent solid potential energy density
$\bar{\psi}^{(f)}$	apparent fluid potential energy density
$\psi^{(f)}$	microscale fluid potential energy density
$\hat{\psi}^{(f)}$	true fluid strain energy density
$\bar{\mathbf{b}}^{(s,ext)}$	solid external volume forces
$\bar{\mathbf{b}}^{(f,ext)}$	fluid external volume forces
$\bar{\mathbf{b}}^{(fs)}$, $\bar{\mathbf{b}}^{(sf)}$	drag volume forces associated with solid-fluid interaction
$\check{\sigma}^{(s)}$	extrinsic solid stress tensor
$\hat{p}^{(s)}$	intrinsic solid pressure
$\boldsymbol{\sigma}^{(s)}$	Cauchy stress tensor
p	interstitial fluid pressure
$\mathbf{t}^{(ext)}$	external boundary traction vector (current configuration)
$\boldsymbol{\sigma}^{(ext)}$	external stress tensor
$\check{\boldsymbol{\sigma}}_h^{(s)}$	value attained by the extrinsic stress tensor in a region with uniform stress state
p_h	value attained by the fluid pressure in a region with uniform stress state
$\Omega^{(h)}$	macroscopic space region with uniform stress state
$\Omega^{(u)}$	macroscopic space region undergoing undrained flow conditions
$\bar{\boldsymbol{\varepsilon}}_{dev}^{(s)}$	deviatoric part of the infinitesimal extrinsic strain tensor
$\bar{\boldsymbol{\varepsilon}}_{sph}^{(s)}$	spherical part of the infinitesimal extrinsic strain tensor
$\bar{\boldsymbol{K}}_{iso}^{(s)}$	extrinsic-intrinsic coupling stiffness matrix for isotropic linear materials
$\bar{\boldsymbol{C}}_{iso}^{(s)}$	extrinsic-intrinsic coupling compliance matrix for isotropic linear materials
$\bar{\psi}_{dev}^{(s)}$	deviatoric part of the strain energy of the solid phase in isotropic materials
$\bar{\psi}_{sph}^{(s)}$	spherical part of the strain energy of the solid phase in isotropic materials
$\bar{K}^{\bar{e}^{(s)}\bar{e}^{(s)}}$	$\bar{e}^{(s)}$-associated entry of $\bar{\boldsymbol{K}}_{iso}^{(s)}$
$\bar{K}^{\hat{e}^{(s)}\bar{e}^{(s)}}$	off-diagonal entry of $\bar{\boldsymbol{K}}_{iso}^{(s)}$
$\bar{K}^{\hat{e}^{(s)}\hat{e}^{(s)}}$	$\hat{e}^{(s)}$-associated entry of $\bar{\boldsymbol{K}}_{iso}^{(s)}$
$\bar{K}_{dev}^{(s)}$	deviatoric stiffness modulus in isotropic materials
$\check{\boldsymbol{\sigma}}_{dev}^{(s)}$	deviatoric part of the extrinsic stress tensor
$\check{\boldsymbol{\sigma}}_{sph}^{(s)}$	spherical part of the extrinsic stress tensor

Table 3: List of symbols

Symbol	Description
$\breve{p}^{(s)}$	pressure content of the extrinsic stress tensor
$\bar{k}_V$	macroscopic bulk modulus of the dry solid phase
$\bar{\mu}$	macroscopic shear modulus of the solid phase
$\bar{\lambda}$	macroscopic Lamè modulus of the dry solid phase
$\bar{E}$	macroscopic Young modulus of the dry solid phase
$\bar{\nu}$	macroscopic Poisson ratio of the dry solid phase
$\bar{k}_V$	macroscopic bulk modulus of the dry solid phase
$\hat{k}_r$	dimensionless extrinsic-intrinsic coupling modulus (hat version)
$\bar{k}_r$	dimensionless extrinsic-intrinsic coupling modulus (bar version)
$\hat{k}_s$	solid intrinsic stiffness
$\hat{k}_f$	fluid intrinsic stiffness
$\hat{k}_{sf}$	series coupling modulus of intrinsic solid and fluid stiffness
$\mathbf{w}^{(fs)}$	relative solid-fluid velocity
K	inverse permeability coefficient
κ	intrinsic permeability
$\mu^{(f)}$	effective fluid viscosity
μ	microscale shear modulus of the material constituting the solid phase
k_s	microscale bulk modulus of the material constituting the solid phase
ν	microscale Poisson ratio of the material constituting the solid phase
$\partial\Omega_b^{(M)}$	bottom boundary surface of the macroscopic domain of the mixture contained in the compression char
$\partial\Omega_u^{(M)}$	upper boundary surface of the macroscopic domain of the mixture contained in the compression cham
$\partial\Omega_u^{(M)}$	lateral boundary surface of the macroscopic domain of the mixture contained in the compression cham
F_o	compressive force applied in the test
U_o	compressive displacement applied in the test
$\bar{\boldsymbol{\varepsilon}}_h^{(s)}$	constant value of infinitesimal extrinsic strain tensor in a region with uniform deformation state
$\bar{e}_h^{(s)}$	constant value of infinitesimal extrinsic volumetric strain tensor in a region with uniform deformation
α	Biot's coefficient
$\bar{\boldsymbol{\varepsilon}}_{dev}^{(ext)}$	deviatoric part of the external stress tensor
p^{ext}	pressure content of the external stress tensor
B	Skempton's coefficient
B_{iso}	Skempton's coefficient (pressure ratio)
a_q, b_q, c_q	coefficients for curve fitting the nonlinear extrinsic compliance of sandstone specimens

Table 4: List of symbols